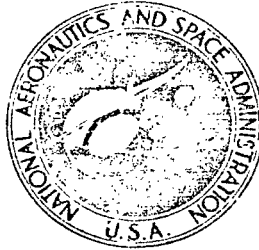


NASA TECHNICAL NOTE

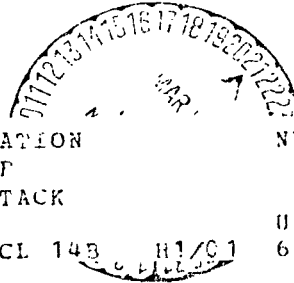


NASA TN D-6986

LOAN COPY  
AFWL TECHN  
KIRTLAND

TECH LIBRARY KAFB, NM  
LIBRARY  
M.  
0133697

NASA TN D-6986



(NASA-TN-D-6986) WIND-TUNNEL CALIBRATION  
AND REQUIREMENTS FOR IN-FLIGHT USE OF  
FIXED HEMISPHERICAL HEAD ANGLE-OF-ATTACK  
AND ANGLE-OF-SIDESLIP SENSORS (NASA)  
47 p HC \$3.00

N73-18014

Unclass  
64504

CSCL 143 H1/C1

WIND-TUNNEL CALIBRATION AND  
REQUIREMENTS FOR IN-FLIGHT USE  
OF FIXED HEMISPHERICAL HEAD  
ANGLE-OF-ATTACK AND  
ANGLE-OF-SIDESLIP SENSORS

by Earl J. Montoya  
Flight Research Center  
Edwards, Calif. 93523



0133697

1. Report No. NASA TN D-6986		2. Government Accession No.		3. Recipient's Catalog No.	
4. Title and Subtitle WIND-TUNNEL CALIBRATION AND REQUIREMENTS FOR IN-FLIGHT USE OF FIXED HEMISPHERICAL HEAD ANGLE-OF-ATTACK AND ANGLE-OF-SIDESLIP SENSORS		5. Report Date March 1973		6. Performing Organization Code	
7. Author(s) Earl J. Montoya		8. Performing Organization Report No. H-702		10. Work Unit No. 761-74-01-00-24	
9. Performing Organization Name and Address NASA Flight Research Center P. O. Box 273 Edwards, California 93523		11. Contract or Grant No.		13. Type of Report and Period Covered Technical Note	
12. Sponsoring Agency Name and Address National Aeronautics and Space Administration Washington, D. C. 20546		14. Sponsoring Agency Code		15. Supplementary Notes	
16. Abstract  <p>Wind-tunnel tests were conducted with three different fixed pressure-measuring hemispherical head sensor configurations which were strut-mounted on a nose boom. The tests were performed at free-stream Mach numbers from 0.2 to 3.6. The boom angle-of-attack range was <math>-6^\circ</math> to <math>15^\circ</math>, and the angle-of-sideslip range was <math>-6^\circ</math> to <math>6^\circ</math>. The test Reynolds numbers were from <math>3.28</math> to <math>65.6 \times 10^6</math> per meter (<math>1.0</math> to <math>20.0 \times 10^6</math> per foot).</p> <p>The results were used to obtain angle-of-attack and angle-of-sideslip calibration curves for the configurations. One configuration, which is being used on the NASA YF-12 airplane, was accurate to <math>\pm 0.25^\circ</math> for angular measurements up to an angle of attack of <math>8^\circ</math> at high supersonic speeds. No significant Reynolds number effects were noted in the results.</p> <p>Signal outputs from the hemispherical head sensor had to be specially processed to obtain accurate real-time angle-of-attack and angle-of-sideslip measurements for pilot displays or aircraft systems. Use of the fixed sensors in flight showed them to be rugged and reliable and suitable for use in a high temperature environment.</p>					
17. Key Words (Suggested by Author(s)) Angle-of-attack sensors Angle-of-sideslip sensors High temperature sensors			18. Distribution Statement  Unclassified - Unlimited		
19. Security Classif. (of this report) Unclassified		20. Security Classif. (of this page) Unclassified		21. No. of Pages 45	22. Price* \$3.00

\* For sale by the National Technical Information Service, Springfield, Virginia 22151

WIND-TUNNEL CALIBRATION AND REQUIREMENTS FOR IN-FLIGHT  
USE OF FIXED HEMISPHERICAL HEAD ANGLE-OF-ATTACK  
AND ANGLE-OF-SIDESLIP SENSORS

Earl J. Montoya  
Flight Research Center

INTRODUCTION

The precise measurement of angle of attack and angle of sideslip is critical for aircraft that cruise at speeds in excess of Mach 3. These parameters are used not only in pilot displays and for obtaining flight-test data but also as inputs for such automatic systems as inlet control, autopilot, and stability augmentation. Vane-type angle-of-attack and angle-of-sideslip sensors were used successfully up to Mach 3 on both the X-15 (refs. 1 and 2) and the XB-70 (ref. 3) aircraft. However, at higher Mach numbers the temperatures to which the electrical sensing elements of the vane are subjected become high enough to affect the reliability of the elements. To overcome this problem, a servo-driven ball nose with pneumatic sensors was used on the X-15 aircraft (refs. 4 and 5). This system kept the pitot port oriented into the relative wind at Mach numbers up to 6.7. The angle of attack and angle of sideslip were measured by sensing the position of the ball. This complex system was necessary because of the large angle-of-attack range through which the airplane flew (refs. 4 and 5). For smaller angle-of-attack ranges, less complex fixed probes of similar design which have the necessary accuracy, response, and linear characteristics throughout the speed and angle-of-attack range are feasible.

Fixed, isolated, hemispherical head sensing probes with static ports  $40^\circ$  to  $45^\circ$  to each side of the axis of symmetry have been tested in wind tunnels. They were found to have linear calibrations of  $\pm 12^\circ$  in the Mach number range from 0.3 to 2.6 (refs. 6 to 8). For practical application on aircraft, it is desirable to mount such flow-direction sensors on the nose boom where the flow is relatively undisturbed.

During the development of the YF-12 hemispherical head angle-of-attack—angle-of-sideslip sensor, three sensor configurations mounted off the nose boom were tested in wind tunnels to obtain a calibration to be used in flight. The tests were conducted over a Mach number range of 0.2 to 3.6. This report presents the results of these tests and discusses the effects of configuration changes on the calibrations. Mechanization of the information from the sensors for use in aircraft systems, pilot displays, and test data recording systems is also discussed.

SYMBOLS

Physical quantities in this report are given in the International System of Units (SI)

and parenthetically in U. S. Customary Units. The measurements were made in Customary Units. Factors relating the two systems are given in reference 9.

$E( )$	error of the parameter in parentheses
$M$	Mach number
$p_s$	surface static pressure on the pitot probe, $N/m^2$ (psia)
$p_T$	nose boom pitot pressure, $N/m^2$ (psia)
$p_{T0}$	free-stream total pressure, $N/m^2$ (psia)
$p_1, p_2, p_3, p_4$	hemispherical head pressures (page 4), $N/m^2$ (psia)
$q_0$	free-stream dynamic pressure, $N/m^2$ (lb/ft <sup>2</sup> )
$N_{Re}$	Reynolds number, per m (per ft)
$\alpha$	nose boom angle of attack, deg
$\alpha_c$	calculated angle of attack, deg
$\beta$	nose boom angle of sideslip, deg
$\beta_c$	calculated angle of sideslip, deg
$\Delta p = \Delta p_\alpha$ or $\Delta p_\beta$ , or both,	$N/m^2$ (psi)
$\frac{\Delta p}{q_0}$	sensor differential pressure coefficient
$\Delta p_\alpha = p_3 - p_1$ ,	$N/m^2$ (psi)
$\Delta p_\beta = p_2 - p_4$ ,	$N/m^2$ (psi)
$\Delta\alpha$	nose boom angle of attack for zero $\frac{\Delta p_\alpha}{q_0}$ , deg
$\Delta\beta$	nose boom angle of sideslip for zero $\frac{\Delta p_\beta}{q_0}$ , deg

## CONFIGURATIONS TESTED

Three-view drawings of the fixed hemispherical angle-of-attack—angle-of-sideslip sensors tested are shown in figures 1(a) to 1(c). The sensors were strut-mounted on a nose boom with a pitot head. Pertinent configuration characteristics are given in table 1. The configurations differed primarily in alinement relative to the airspeed boom and in standoff distance. All three configurations were tested in wind tunnels. Photographs of configuration C, which was flown on the YF-12 aircraft, are shown in figures 2 and 3.

## WIND TUNNELS

Wind-tunnel tests were made in the Lockheed Aircraft Corporation (LAC) 8- by 12-foot low speed wind tunnel and the 4- by 4-foot supersonic tunnel and in the Ames Research Center (ARC) 8- by 7-foot supersonic tunnel. Table 2 lists the pertinent characteristics of these wind tunnels. Additional detail on the LAC 4- by 4-foot and ARC 8- by 7-foot supersonic tunnels are presented in references 10 and 11.

## TEST CONDITIONS

Conditions for the wind-tunnel tests were as follows:

Configuration	Tunnel		$N_{Re}$ per m (per ft)
	LAC		
A			4.92 (1.5) $\times 10^6$
			to
B			4.92 (1.5) $\times 10^6$
			to
C			3.28 (1.0) $\times 10^6$
			to

0    .4    .8    1.2    1.6    2.0    2.4    2.8    3.2    3.6  
M

The configuration C tests conducted by Lockheed were monitored by NASA.

### DATA REDUCTION

Mach number,  $M$ , free-stream dynamic pressure,  $q_0$ , free-stream total pressure,  $p_{T0}$ , and the hemispherical head pressures,  $p_1$ ,  $p_2$ ,  $p_3$ , and  $p_4$ , together with angle of attack and angle of sideslip, were obtained from the wind-tunnel tests. The four hemispherical head pressures obtained are shown in the adjacent sketch.

Differential sensor pressure coefficients,  $\frac{\Delta p_\alpha}{q_0}$  or  $\frac{\Delta p_\beta}{q_0}$ , or both, were calculated by using the following expressions:

$$\frac{\Delta p_\alpha}{q_0} = \frac{p_3 - p_1}{q_0}$$

and

$$\frac{\Delta p_\beta}{q_0} = \frac{p_2 - p_4}{q_0}$$

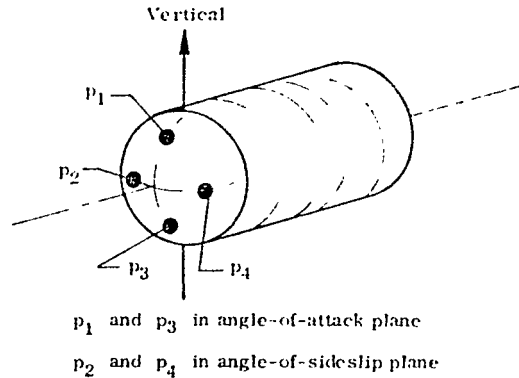
The data for configurations A and B, which were tested by Lockheed, were provided in terms of  $\frac{\Delta p}{p_{T0}}$  versus angle for both angle of attack and angle of sideslip. The ratio

$\frac{p_{T0}}{q_0}$  was determined by using reference 12 for each Mach number tested. Then  $\frac{\Delta p}{q_0}$  was obtained by using the expression

$$\frac{\Delta p}{p_{T0}} \frac{p_{T0}}{q_0} = \frac{\Delta p}{q_0}$$

Configuration C data were provided in the required parameters.

The plots of  $\frac{\Delta p}{q_0}$  versus angle show that the results tend to be linear. The slopes



of the linear results were measured over an increment range through the origin of approximately  $10^\circ$ , which yielded a calibration sensitivity factor of  $\frac{\Delta p}{q_0 \text{ Angle}}$ . The

sensitivity was determined for each Mach number and configuration. Plots of  $\frac{\Delta p}{q_0 \text{ Angle}}$  versus Mach number were made from these results.

### ACCURACY

The accuracy of a flow direction sensor is a function of both the wind-tunnel calibration error and the error associated with the instrumentation used to measure flow direction. The most important information to be obtained from a wind-tunnel calibration

is the change in the differential sensor pressure coefficient,  $\frac{\Delta p}{q_0}$ , per degree of angular change as a function of Mach number. A calibration of this type was developed

which used measured slopes equal to  $\frac{\Delta p}{q_0 \text{ Angle}}$ , in which angle is an increment where the

faired data line was linear. The slope calibration minimized the effects of zero shift and bias errors due either to misalignment of the probe or to deflections of the sting due to air loads during the calibrations. Nonetheless, the probe was alined as carefully as possible in the tunnel, using a transit and an inclinometer. The estimated average errors in tunnel positioning and Reynolds number, absolute pressure, and sensor pressures were as follows:

Parameter	Estimated average error
$\alpha$	$\pm 0.18^\circ$
$\beta$	$\pm 0.11^\circ$
$N_{Re}$	$\pm 0.7 \times 10^6$ per m ( $\pm 0.2 \times 10^6$ per ft)
$p_{T0}$	$\pm 0.25$ percent of reading
$p_1, p_2,$ $p_3, p_4$	$\pm 344.7$ N/m <sup>2</sup> ( $\pm 0.05$ psi)

The error in Mach number became larger with increasing Mach number, as shown in the following tabulation:

M	E(M)
0.2	± 0.001
.7	± .003
.9	± .004
.95	± .004
1.0	± .004
1.05	± .004
1.1	± .004
1.4	± .007
2.0	± .010
2.6	± .020
3.2	± .060
3.6	± .080

To apply the calibration,  $\frac{\Delta p}{q_0}$  was determined at a particular Mach number from the pressures measured by a properly aligned probe and divided by the calibration factor as follows:

$$\text{Angle} = \frac{\left(\frac{\Delta p}{q_0}\right)_{\text{measured}}}{\left(\frac{\Delta p}{q_0}\right)_{\text{calibration}}}$$

The portion of the angular error attributed to the calibration factor was caused by the tunnel positioning and pressure errors mentioned previously. The effects of these position and pressure errors on the slope calibration and the resultant angular error were calculated using the techniques of reference 13. (The error in the measured

$\frac{\Delta p}{q_0}$  is a function of the installation and therefore is not included.)

The errors resulting from the effect of Mach number errors on  $q_0$  and  $\frac{q_0}{p_{T0}}$  were used to obtain the overall error shown in figures 4(a) and 4(b). Since the values of  $\frac{\Delta p}{q_0 \text{ measured}}$  and  $\frac{\Delta p}{p_{T \text{ measured}}}$  can vary over a wide range (angles of attack from  $-1^\circ$  to  $16^\circ$  and angles of sideslip from  $-5^\circ$  to  $5^\circ$ ) in the subsonic to supersonic Mach number range, the calibration errors are presented as a percentage of the angle-of-attack and angle-of-sideslip readings. These errors were 3 percent or less at the high supersonic Mach numbers. In this airspeed range, angle of attack and angle of sideslip were normally less than  $8^\circ$ , which resulted in calibration angular measurements that were accurate within  $\pm 0.25^\circ$  (approximately  $8^\circ \times 0.03$ ).

## RESULTS AND DISCUSSION

Configuration C was chosen for use on the NASA YF-12 airplane for several reasons. An accurate airspeed and angle-of-attack — angle-of-sideslip indication system was desired to provide critical airspeed and flight information to both the pilot and the aircraft systems over the operating range. Emphasis was placed on operation at high supersonic Mach numbers. The alignment of the hemispherical head to the flow at flight angles of attack governed the design of configurations B and C. As is shown, all three configurations would have been adequate for obtaining the angle of attack and angle of sideslip. However, interactions between the strut-mounted fixed hemispherical head sensor and the airspeed pitot head also had to be considered. These interactions were minimized in configuration C.

Wind-tunnel results for all the configurations tested are presented in figures 5 to 13. Samples of the basic data in terms of the sensor pressure coefficient versus angle of attack and sideslip are plotted in figures 5, 8, and 11 for the Mach numbers tested. The calibration for angle-of-attack and angle-of-sideslip curves is generally linear from  $-6^\circ$  to  $8^\circ$  about the zero pressure coefficient. Minor nonlinearities occur outside this range.

A summary of the sensitivity, or  $\frac{\Delta p}{q_0 \text{ Angle}}$ , of the basic calibration curves in figures 5, 8, and 11 is shown as a function of Mach number in figures 6, 9, and 12. A sharp drop in  $\frac{\Delta p}{q_0}$  occurs in the transonic region (figs. 6 and 9) followed by a gradual rise as Mach number increases. It should be noted that as  $\frac{\Delta p}{q_0 \text{ Angle}}$  decreases, the sensitivity of the angle calculated (or the resolution of the angle) for the pressure coefficient measured increases. Therefore, in the transonic region and up to Mach 1.8 errors in  $\left(\frac{\Delta p}{q_0}\right)_{\text{measured}}$  or Mach number can result in a significant angular error.

The calibrations tend to become constant again above Mach 2.6.

No significant Reynolds number effects were apparent in the Reynolds number range from  $3.28$  to  $65.6 \times 10^6$  per meter ( $1.0$  to  $20.0 \times 10^6$  per foot) (figs. 11(b) and 11(d)).

Because of the inclination of the angle-of-attack probes and ports to the nose boom centerline, the coefficient of differential sensor pressure should be zero at angles of attack of  $0^\circ$ ,  $4^\circ$ , and  $3.4^\circ$  for the A, B, and C configurations, respectively. The coefficient of differential sensor pressure should be zero at a sideslip angle of  $0^\circ$  for all the configurations tested. Deviations from the theoretical zero pressure coefficient crossings shown in figures 5, 8, and 11 are attributed to a combination of flow conditions around the probe, tunnel flow angularities, and tunnel measurement tolerances.

Figures 7, 10, and 13 show the angles ( $\Delta\alpha$  and  $\Delta\beta$ ) that correspond to zero pressure coefficients for configurations A, B, and C, respectively.

### Configuration A

The wind-tunnel results for configuration A are presented in figures 5, 6, and 7. Individual fairings of the angle-of-attack and angle-of-sideslip data were made; however,

scatter in the supersonic slope data,  $\frac{\Delta p}{q_0}$ , indicates that a single fairing to represent the  $\alpha$  and  $\beta$  variations (fig. 6) may be appropriate, depending on the accuracy required. For use on an aircraft, the error caused by using a single curve rather than individual angle-of-attack and angle-of-sideslip curves was evaluated by determining the difference between the angles in the individual calibration curves and those in the faired curve. The following table shows typical biased errors which result from using a single curve:

Mach number	Typical angle of attack, deg	Error in angle of attack, deg
0.4	7	0.11
1.0	2	.05
1.4	6	.18
2.0	6	.15
2.6	6	.13
3.0	4	.08
3.6	4	.08

Normally the angle of sideslip is within  $\pm 1^\circ$ , so the biased error in the angle of sideslip would be about  $-0.03^\circ$ . The difference between the faired curve and the angle-of-sideslip curve is about 3 percent over the Mach range. Because these errors are biased, they can be corrected for; however, the use of the individual calibration curves is more accurate. When a single calibration curve is used, results from figure 4 and the biased errors would be used to determine the total calibration error in angle of attack and angle of sideslip.

The angles at which the intersection point for angle of attack ( $\Delta p_\alpha = 0$ ) and angle of sideslip ( $\Delta p_\beta = 0$ ) occurred are shown in figure 7. As shown, the intersection points are not at  $0^\circ$ . The following angular corrections ( $\Delta\alpha$  and  $\Delta\beta$ ) should be applied to obtain an accurate angle determination:

$$\alpha = \Delta\alpha + \frac{\left(\frac{\Delta p}{q_0}\right)_{\text{measured}}}{\left(\frac{\Delta p}{q_0}\right)_{\text{calibration}}}$$

and

$$\beta = \Delta\beta + \frac{\left(\frac{\Delta p}{q_0}\right)_{\text{measured}}}{\left(\frac{\Delta p}{q_0}\right)_{\text{Angle}}}_{\text{calibration}}$$

### Configuration B

Figures 8, 9, and 10 present the wind-tunnel results for configuration B. The fairings of the sensitivity factor versus Mach number data at the lower Mach numbers

(fig. 9) are based on the fairings in figure 6. The values of  $\frac{\Delta p}{q_0 \text{ Angle}}$  at Mach 2.0 and above are lower than those of configuration A and are the result of aligning the hemispherical head sensor 4° downward from the horizontal.

The use of a single calibration curve, determined by fairing through the data of figure 9, to determine angles of attack and sideslip was evaluated. The following table shows the resultant error in angle of attack:

Mach number	Typical angle of attack, deg	Error in angle of attack, deg
0.4	7	0.13
1.0	2	.05
1.4	6	.17
2.0	6	.14
2.6	6	.14
3.0	4	.09
3.2	4	.09

The biased error in angle of sideslip is about -0.03° for nominal angles of sideslip of ±1°.

The corrections for the intersection points for configuration B, which make it possible to obtain accurate angle measurements, are shown in figure 10.

### Configuration C

Figures 11, 12, and 13 present the wind-tunnel results obtained with configuration C.

The values of differential sensor pressure coefficient for both angle of attack and angle of sideslip from the two different tunnels agreed at Mach 2.6 (fig. 11(b)) and Mach 3.2 (fig. 11(d)).

The results from each wind tunnel were plotted separately in terms of the sensitivity

factor,  $\frac{\Delta p}{q_0 \text{ Angle}}$ , versus Mach number (fig. 12). A pronounced difference of approximately 0.0060 in the sensitivity parameter appeared between the angle-of-attack and angle-of-sideslip data for configuration C, presumably because the angle-of-attack ports were shifted asymmetrically downward on the probe face and because it was in a dif-

ferent flow field. This difference in  $\frac{\Delta p}{q_0 \text{ Angle}}$ , which appears to be nearly constant over

the Mach number range tested, is confirmed by the LAC and ARC results. The  $\frac{\Delta p_\beta}{q_0 \text{ Angle}}$  of the angle-of-sideslip slope is less than that of the angle-of-attack slope at any given Mach number.

Use of the single calibration curve shown in figure 12 to determine both angle of attack and angle of sideslip would result in the biased errors shown in the table below. Reynolds number differences did not seem to affect the results (figs. 11(b) and 11(d)).

Mach number	Typical angle of attack, deg	Error in angle of attack, deg
1.4	6	0.32
2.0	6	.32
2.6	6	.27
3.0	4	.25
3.2	4	.29
3.4	4	.20

The biased error in sideslip for a nominal angle of sideslip of 1° is approximately -0.06°. Intersection point corrections ( $\Delta\alpha$  and  $\Delta\beta$ ) for this configuration are presented in figure 13. Below Mach 1.4 the fairing was based on subsonic results for configurations A (fig. 7) and B (fig. 10), because no subsonic data were taken for configuration C. The angle-of-sideslip correction is essentially zero for Mach numbers greater than 1.4.

## Comparisons

Because no data were obtained below Mach 1.4 for configuration C, a means of obtaining a calibration curve from Mach 0.2 to 1.4 was needed. The results from all three configurations are combined in figure 14. This figure was used to generate an angle-of-attack—angle-of-sideslip calibration curve over the entire Mach range for configuration C.

Comparison of angle-of-attack data. — The angle-of-attack results for all three configurations are shown in figure 14(a). In general, data for configurations A and B agree

within  $\pm 0.003 \frac{\Delta p_{tot}}{q_0}$  over the Mach range from 0.2 to 2.2. All three configurations are in general agreement from Mach 1.4 to 2.2. Above Mach 2.2, the data for configurations A and C agree within  $\pm 0.003$  in sensitivity, but the configuration B results are low. A full-range calibration for configuration C was generated by taking into consideration the results of configurations A and B in the Mach number range from 0.2 to 1.4, and those of configuration C in the Mach number range from 1.4 to 3.6.

Comparison of angle-of-sideslip data. — Figure 14(b) is a compilation of the angle-of-sideslip-determined sensitivities from the configurations tested. Configurations A and B show that the angle-of-sideslip results differ from the angle-of-attack results by a constant (angle-of-sideslip sensitivity was approximately 0.003 lower than angle-of-attack sensitivity) over the Mach number range (figs. 6 and 9). A calibration curve for the angle-of-sideslip data for configuration C was faired using the general shape characteristics of the angle-of-sideslip data calibration curve in the Mach number range from 0.2 to 1.4. Above Mach 1.4, the calibration curve fairing was weighted by the configuration C angle-of-sideslip data.

## Mechanization of Calibration Curves

Because angle of attack and angle of sideslip are important flight parameters for pilot display and input elements into automatic systems, a means of obtaining these values quickly and accurately on board an aircraft would be desirable. Since fixed hemispherical head sensors do not provide a direct readout of angle of attack or angle of sideslip, special processing of the hemispherical head sensor data is necessary.

Although dynamic pressure,  $q_0$ , is a fundamental parameter in the calibration

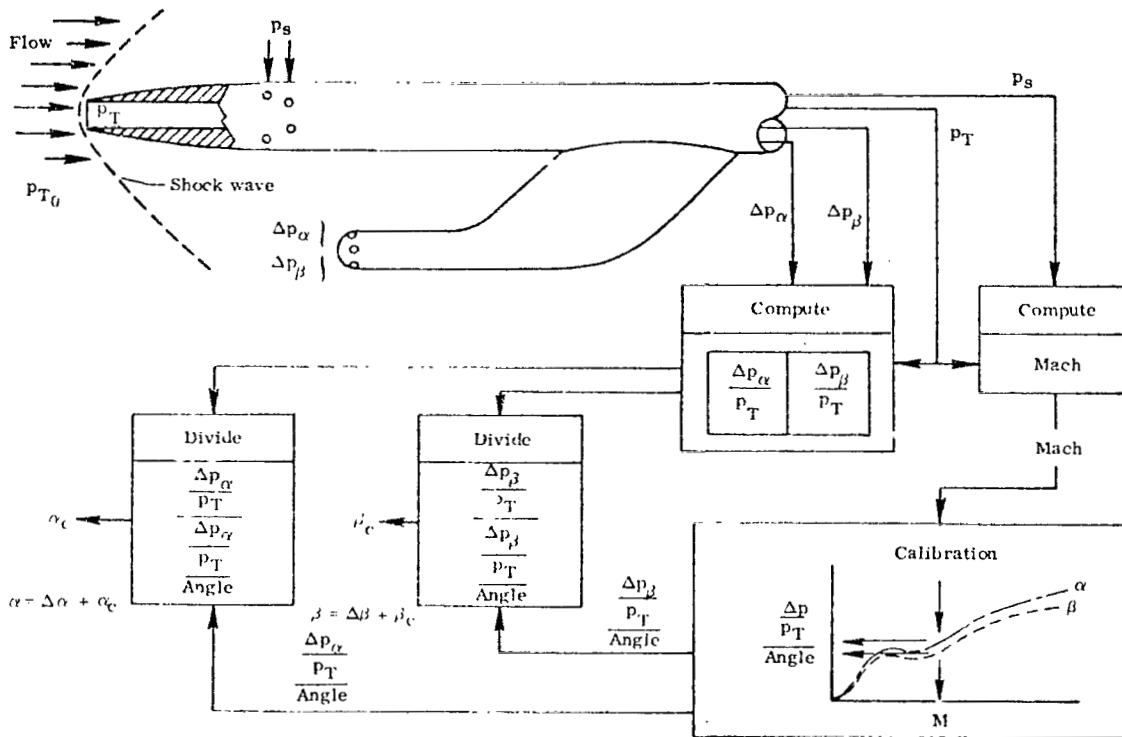
term,  $\frac{\Delta p}{q_0 \text{ Angle}}$ , it is not easily measured in flight. Therefore, an alternate technique using nose boom pitot pressure,  $p_T$ , for the angle-of-attack—angle-of-sideslip calibration instead of  $q_0$  has been developed for use on an aircraft.

A plot of  $\frac{q_0}{p_T}$  versus Mach number is presented in figure 15. This figure presents

theoretical results obtained from reference 12 and typical flight-test results obtained with configuration C. As shown, the theoretical results and the test data generally agree and above Mach 1.8 tend to become less sensitive to Mach number changes. Using the results shown in figure 15 and the calibration curves shown in figure 14, a

calibration was obtained in terms of  $\frac{\Delta p}{p_T}$  (fig. 16). The data flow diagram

associated with the  $\frac{\Delta p}{p_T}$  calibration curves is shown in the following schematic drawing:



This schematic also illustrates a technique developed (using  $\frac{\Delta p}{p_T}$ ) to present angle of attack and angle of sideslip to the pilot in flight. A constant intersection correction for  $\Delta\alpha$  and  $\Delta\beta$  is assumed and applied. To accomplish this, an air-data computer would be used to provide indicated Mach number from  $p_T$  and  $p_s$ . A high-speed

onboard digital computer would store the calibration and perform the tasks shown in the data flow diagram. Inputs to this computer would be  $\Delta p_\alpha$ ,  $\Delta p_\beta$ ,  $p_T$ , and indicated Mach number. The outputs from the computer would drive angle-of-attack and angle-of-sideslip indicators. An installation of this type was flown on the NASA YF-12 airplane with the configuration C sensor at Mach numbers up to 3.0 and temperatures in excess of 290° C (550° F).

## APPLICATIONS

The fixed hemispherical sensors tested offer improved reliability, since they had no moving parts and, unlike conventional vane-type sensors, did not require a minimum aerodynamic torque or flutter speed. This was especially advantageous at high Mach numbers. In addition, the sensors were rugged and required little maintenance once installed. They did require an onboard computer to provide real-time pilot displays, and pressure lag effects had to be considered if long pressure lines were used or if dynamic response was desired.

The device would lend itself to use on highly maneuverable aircraft, since it appeared to be insensitive to high g loads (boom bending excluded). High temperature and vibration did not appear to affect the sensor adversely. The sensor could also have been used as an in-flight research probe to study flow characteristics at locations other than the airspeed boom area, such as inside the inlet.

In an inlet application, an isolated hemispherical head sensor would be used (rather than a nose boom or pitot probe like configuration C). A comparison of isolated probe results from various studies with configuration C sensor results is shown in figure 17. Only angle-of-attack results are compared. The pressure orifices in all the isolated probes except those discussed in reference 14 were located 45° relative to the sensor axis. The isolated probe data were corrected to obtain an equivalent  $p_T$  by using the technique suggested in reference 12. As expected, agreement is good at subsonic speeds and through the transonic region. However, with increasing speeds the results diverge. This divergence is believed to be generated by the pitot head flow field. The flow field effects are negligible through the low supersonic speeds but become more pronounced at higher supersonic speeds.

## CONCLUSIONS

Wind-tunnel pressure tests of three full-scale fixed hemispherical angle-of-attack and angle-of-sideslip sensor probes mounted off a nose boom were made over the free-stream Mach number range from 0.2 to 3.6 to obtain a calibration for flight use. The test data provided angle-of-attack and angle-of-sideslip calibrations for each of the sensor configurations and led to the following conclusions:

1. Angular measurements accurate to  $\pm 0.25^\circ$  were possible for angles up to  $8^\circ$  at high supersonic speeds. Errors at transonic speeds could have been considerably larger.

2. A single calibration curve for determining both angle of attack and angle of sideslip could have been used in conjunction with appropriate bias error corrections. Reynolds number effects were negligible for the range of values tested.

3. The fixed sensors were rugged and reliable with no moving parts; however, pneumatic lag due to line length had to be considered. Flight experience showed these devices to be suitable for use in a high temperature environment.

4. In-flight onboard hemispherical head sensor signal outputs required special processing to obtain accurate real-time angle-of-attack and angle-of-sideslip measurements that were satisfactory for pilot displays or aircraft systems.

5. The results from boom-mounted probe tests showed good agreement with results from tests of probes in an isolated mounting up to a Mach number of 1.4 but poor agreement at higher speeds, probably because of the proximity of the pitot head and boom.

Flight Research Center,

National Aeronautics and Space Administration,

Edwards, Calif., September 8, 1972.

## REFERENCES

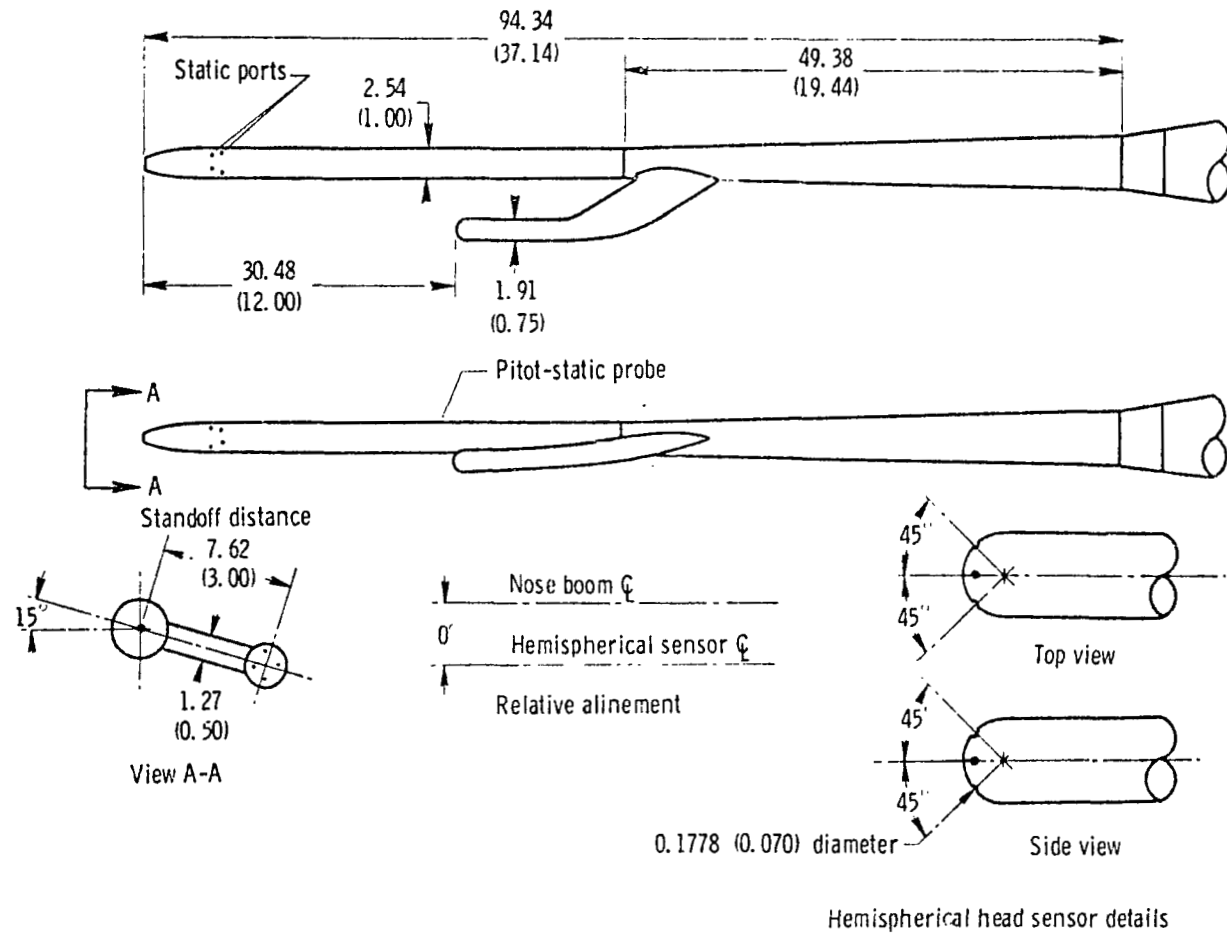
1. Stillwell, Wendell H.; and Larson, Terry J.: Measurement of the Maximum Altitude Attained by the X-15 Airplane Powered With Interim Rocket Engines. NASA TN D-623, 1960.
2. Fischel, Jack; and Webb, Lannie D.: Flight-Informational Sensors, Display, and Space Control of the X-15 Airplane for Atmospheric and Near-Space Flight Missions. NASA TN D-2107, 1964.
3. Wilson, Ronald J.; Love, Betty J.; and Larson, Richard R.: Evaluation of Effects of High-Altitude Turbulence Encounters on the XB-70 Airplane. NASA TN D-6457, 1971.
4. Wolowicz, Chester H.; and Gossett, Terrence D.: Operational and Performance Characteristics of the X-15 Spherical, Hypersonic Flow-Direction Sensor. NASA TN D-3070, 1965.
5. Cary, John P.; and Keener, Earl R.: Flight Evaluation of the X-15 Ball-Nose Flow-Direction Sensor as an Air-Data System. NASA TN D-2923, 1965.
6. Hutton, P. G.: Static Response of a Hemispherical-Headed Yawmeter at High Subsonic and Transonic Speeds. C. P. No. 401, British A. R. C., 1958.
7. Roberts, B. G.: Static Response of Hemispherical Headed, Differential Pressure Incidencemeter From  $M = 1.6$  to  $2.6$ . Tech. Note HSA 43, Weapons Research Establishment, Australian Defence Scientific Service, Nov. 1959.
8. Smetana, Frederick O.; and Headley, Jack W.: A Further Study of Angle-of-Attack Angle-of-Sideslip Pitot-Static Probes. WADC Tech. Rep. 57-234 Part II. Wright Air Development Center, June 1958. (Available from DDC as AD 151089.)
9. Mechtly, E. A.: The International System of Units - Physical Constants and Conversion Factors. NASA SP-7012, 1969.
10. Anon.: The Lockheed 4-Ft.  $\times$  4-Ft. Supersonic Wind Tunnel - Technical Description. Rep. No. C-1-II, Lockheed Gas Dynamics Laboratory.
11. Staff of the Ames Research Center: Research Facilities Summary. Vol. II-Wind Tunnels. Subsonic, Transonic and Supersonic. NASA, Dec. 1965.
12. Kerr, H. C.: Mach Number Tables ( $\gamma = 1.4$ ) With Correction Factors for Real Air. CM 1036-1, Ordnance Aerophysics Lab. (Daingerfield, Tex.), General Dynamics, April 9, 1964. (Available from DDC as AD 624598.)
13. Barry, B. Austin: Engineering Measurements. John Wiley & Sons, Inc., 1964.
14. Beecham, L. J.; and Collins, S. J.: Static and Dynamic Response of a Design of Differential Pressure Yawmeter at Supersonic Speeds. C. P. No. 414, British A. R. C., 1958.

TABLE 1. CONFIGURATION CHARACTERISTICS

Nose boom length, cm (in.) . . . . .	94.34 (37.14)		
Sensor head diameter, cm (in.) . . . . .	1.91 (0.75)		
Pressure port diameter (on sensor head), cm (in.) . . . . .	0.178 (0.07)		
Strut-			
Thickness, cm (in.) . . . . .	1.27 (0.50)		
Shape . . . . .	Biconvex airfoil		
Deflection of hemispherical sensor head below horizontal centerline, deg . . . . .	15		
Sensor port plane-			
Angle of attack . . . . .	Vertical		
Angle of sideslip . . . . .	Horizontal		
	Configuration		
	A	B	C
Strut standoff distance, cm (in.) . . . . .	7.62 (3.00)	6.30 (2.48)	6.35 (2.50)
Distance of sensor from tip, cm (in.) . . . . .	30.48 (12.00)	30.48 (12.00)	32.71 (12.88)
Sensor centerline alignment, deg . . . . .	0	4	0
Location of ports-			
Angle of attack . . . . .	45° from sensor centerline	45° from sensor centerline	Offset 3.4 downward (90° apart)
Angle of sideslip . . . . .	45° from sensor centerline	45° from sensor centerline	45° from sensor centerline

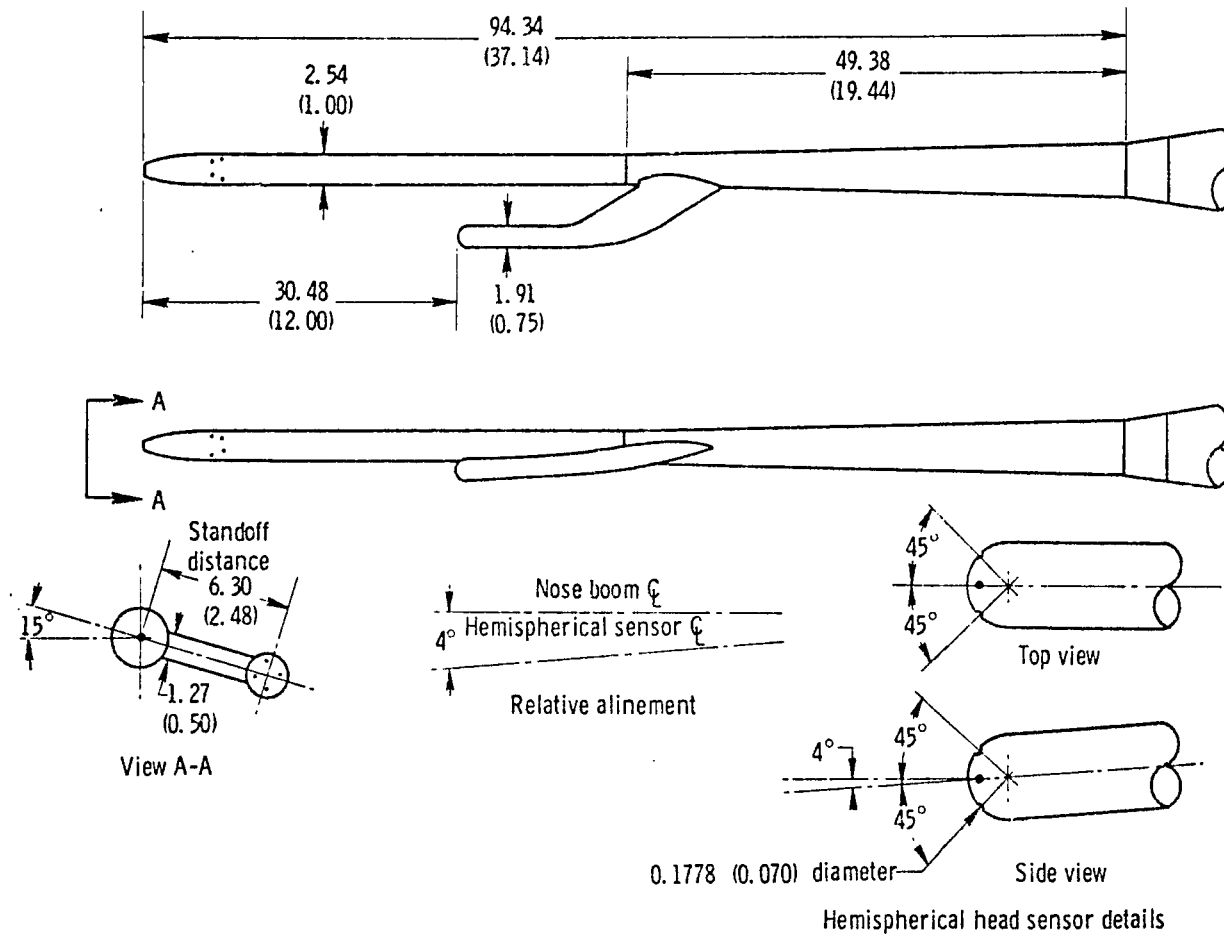
TABLE 2. PERTINENT WIND-TUNNEL CHARACTERISTICS

LAC 8- by 12-foot low speed wind tunnel-	
Operation . . . . .	Continuous, closed-circuit
Mach number . . . . .	0 to 0.30
Reynolds number . . . . .	Up to $6.56 \times 10^6$ per meter ( $2.0 \times 10^6$ per foot)
Normal angularity testing capability, deg:	
Angle of attack . . . . .	-10 to 20
Angle of sideslip . . . . .	-30 to 30
Propeller for airflow-	
Type . . . . .	Six-bladed (wooden)
Diameter, m (ft) . . . . .	6.10 (20)
Power, MW (hp) . . . . .	1.86 (2500)
LAC 4- by 4-foot supersonic wind tunnel-	
Operation . . . . .	Blow-down; pressure storage with atmospheric exhaust
Mach number . . . . .	0.7 to 5.0
Reynolds number . . . . .	Up to $65.6 \times 10^6$ per meter ( $20 \times 10^6$ per foot)
Normal stagnation pressure, N/m <sup>2</sup> (psia) . . . . .	$4.137 \times 10^6$ (600)
Stagnation temperature, °K (°R) . . . . .	311.0 to 394.3 (559.7 to 709.7)
Running time, sec . . . . .	5 to approximately 180
ARC 8- by 7-foot supersonic wind tunnel-	
Operation . . . . .	Continuous flow
Mach number . . . . .	2.45 to 3.5
Reynolds number . . . . .	$3.28$ to $16.4 \times 10^6$ per meter ( $1.0$ to $5.0 \times 10^6$ per foot)
Stagnation pressure, N/m <sup>2</sup> (psia) . . . . .	$3.04$ to $20.26 \times 10^4$ (4.41 to 29.4)
Stagnation temperature, °K (°R) . . . . .	322.5 (580)



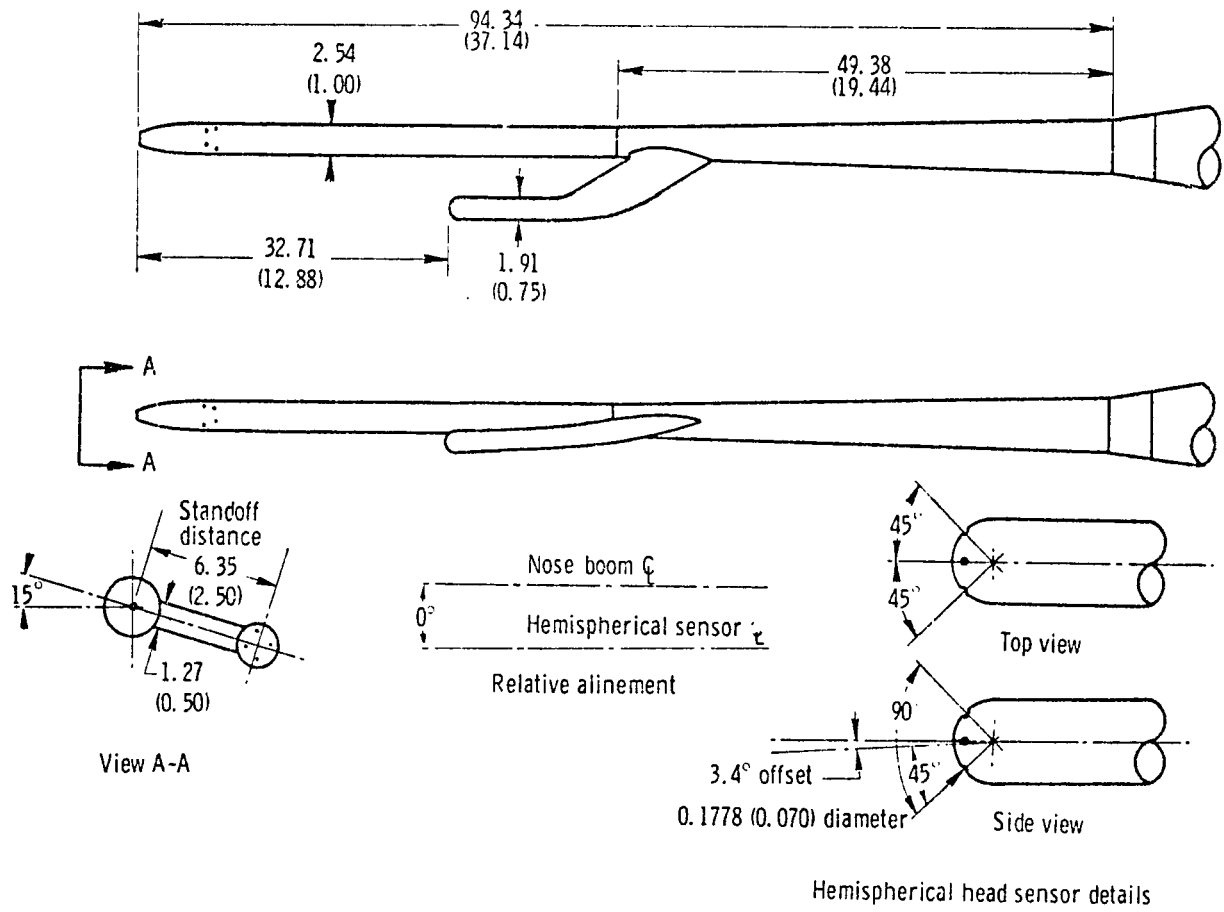
(a) Sensor configuration A.

Figure 1. Three-view drawing of nose boom and pitot-static probe showing strut-mounted hemispherical head angularity sensor. Dimensions in centimeters (inches) except as otherwise noted.



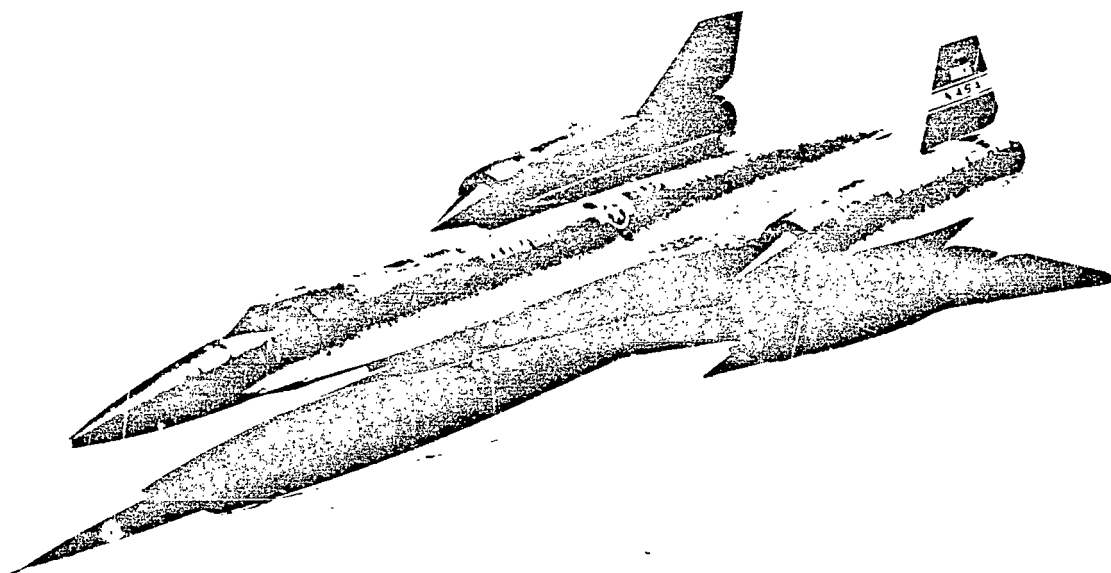
(b) Sensor configuration B.

Figure 1. Continued.



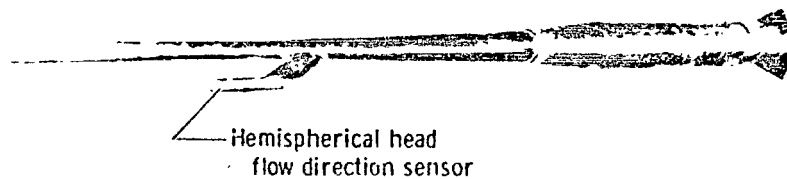
(c) Sensor configuration C.

Figure 1. Concluded.



(a) Test airplane.

E-23129



(b) Pitot-static probe.

Figure 2. Photograph of configuration C, which is being flown on the YF-12 aircraft.

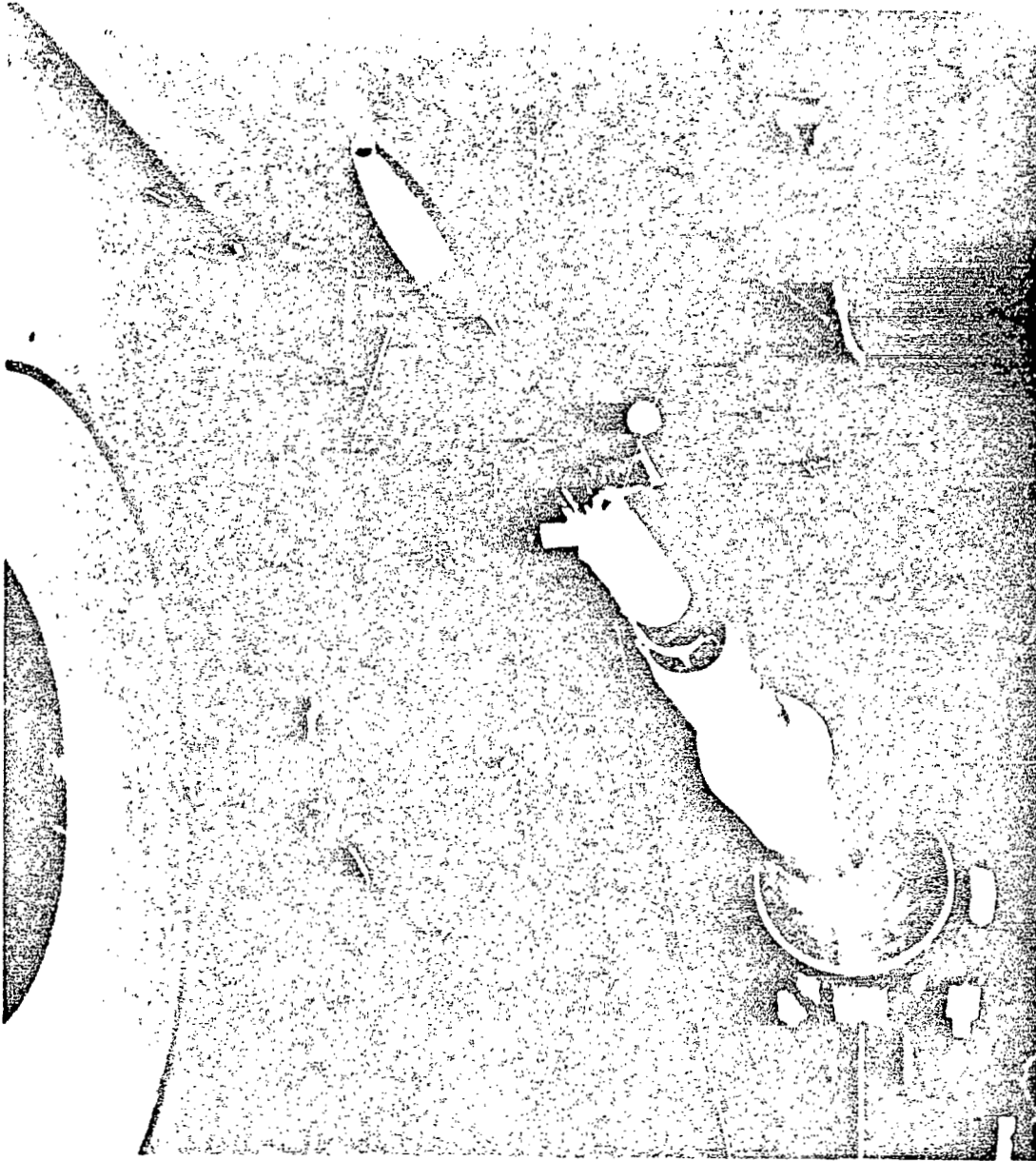
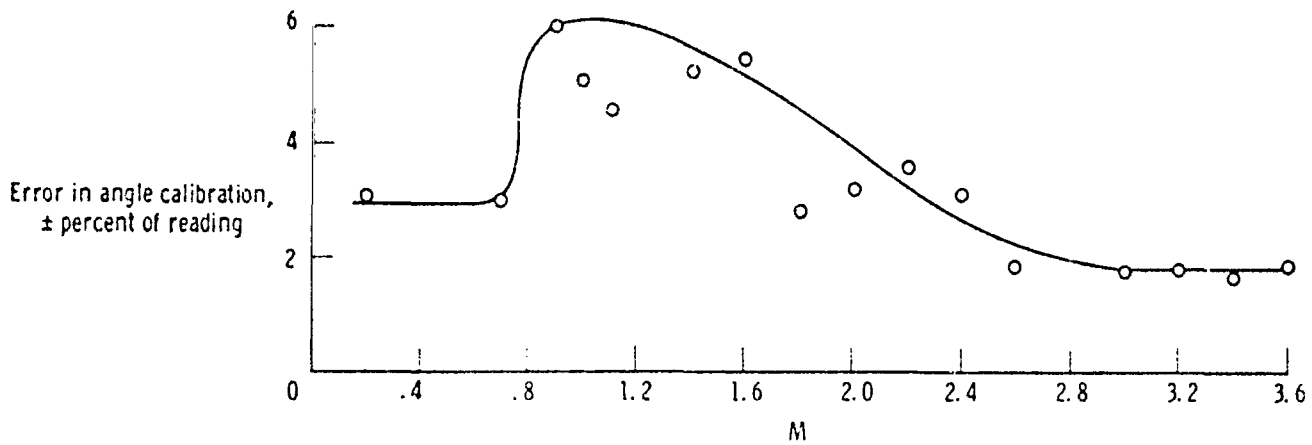
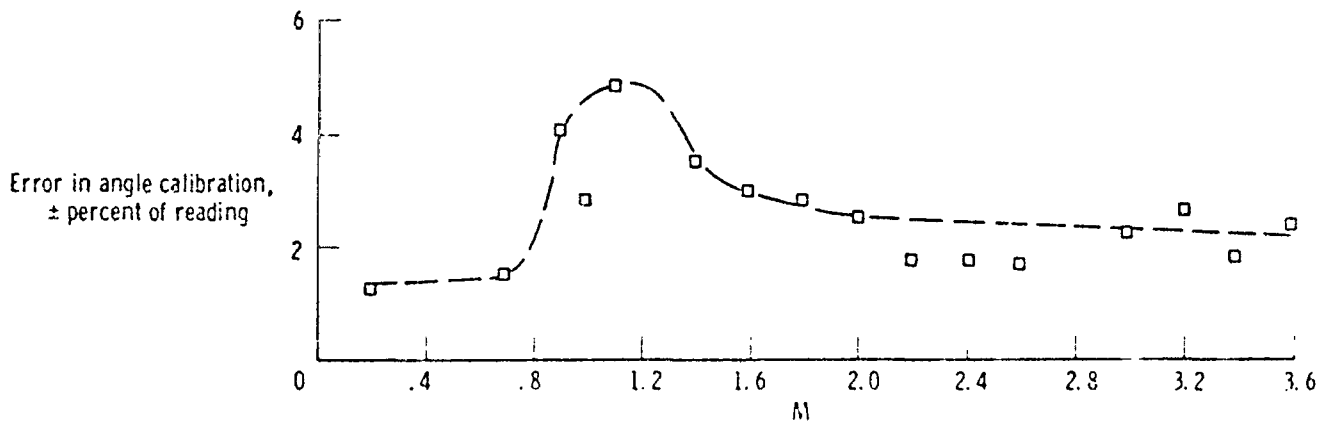


Figure 3. Configuration C mounted in the ARC wind tunnel. A-41704

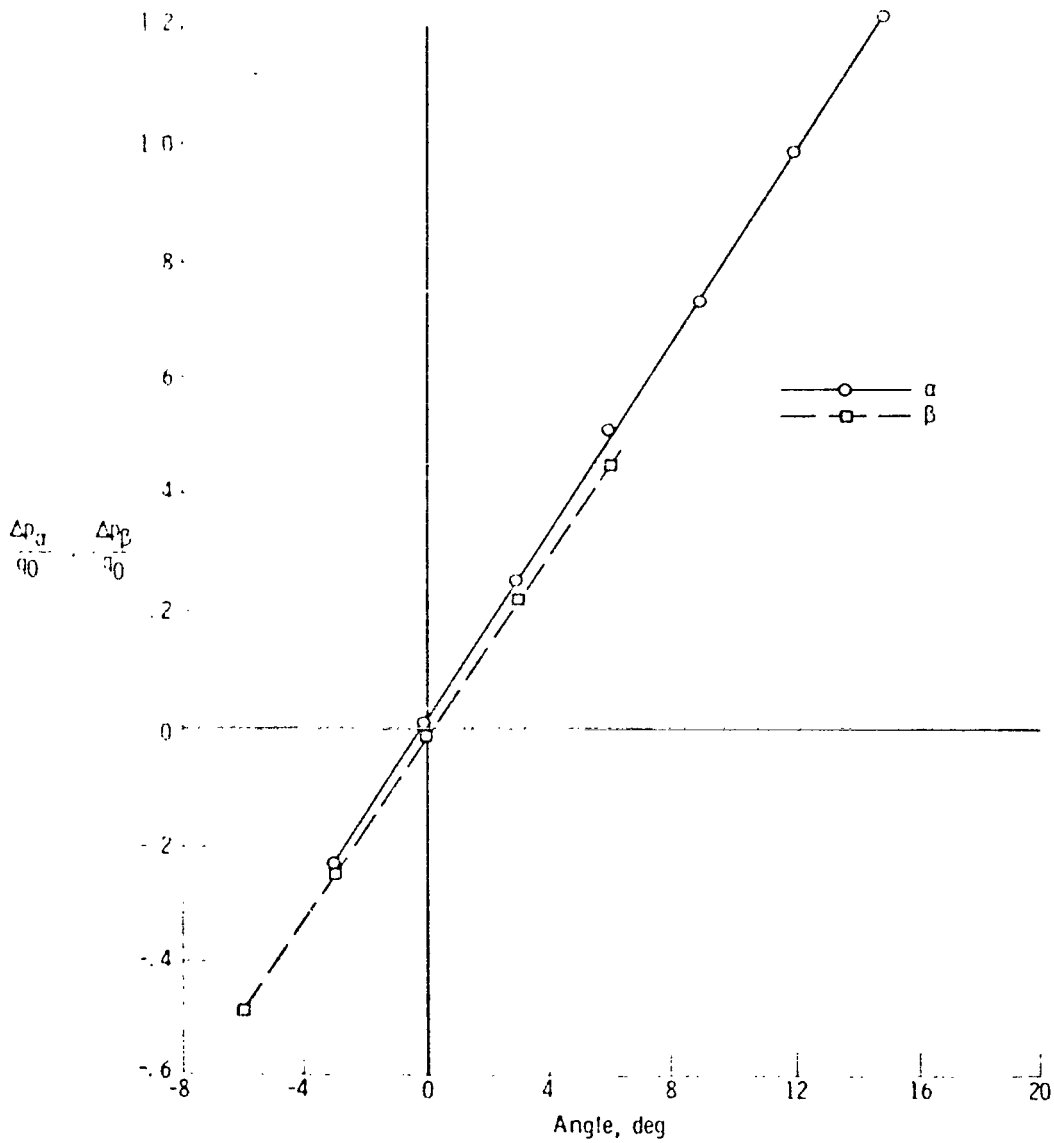


(a) Angle of attack.



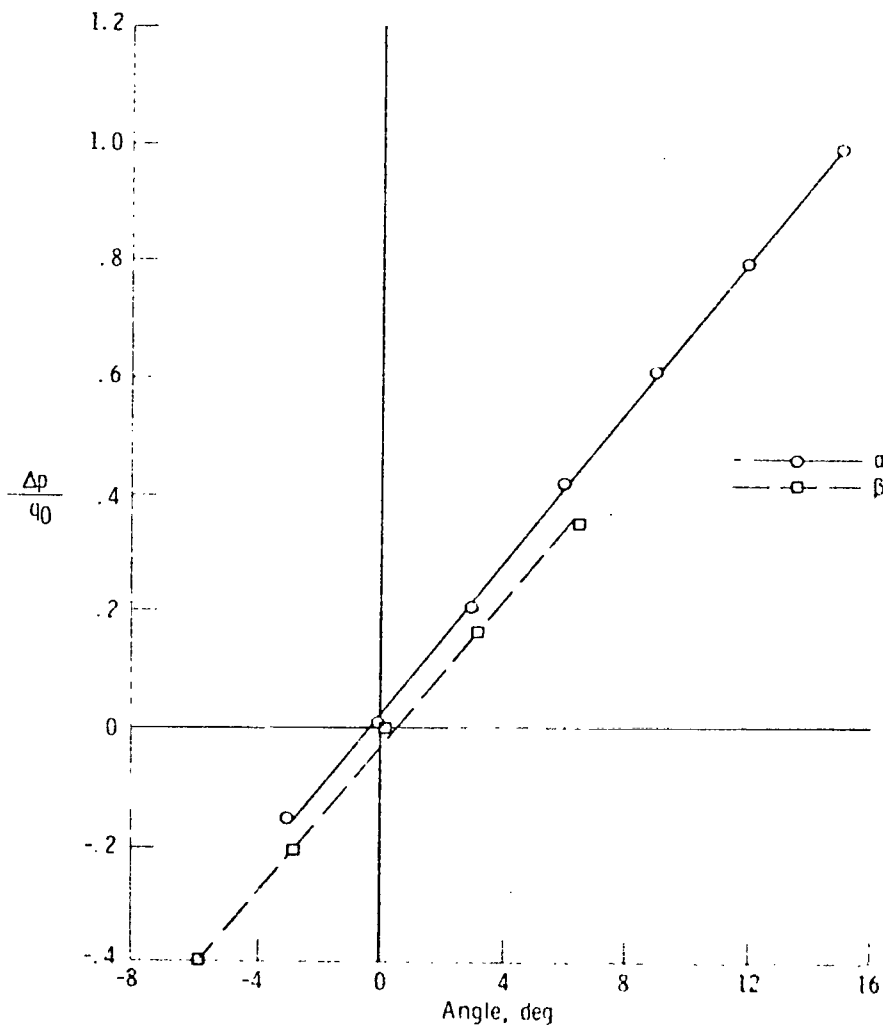
(b) Angle of sideslip.

Figure 4. Estimated error in calibration slopes used.



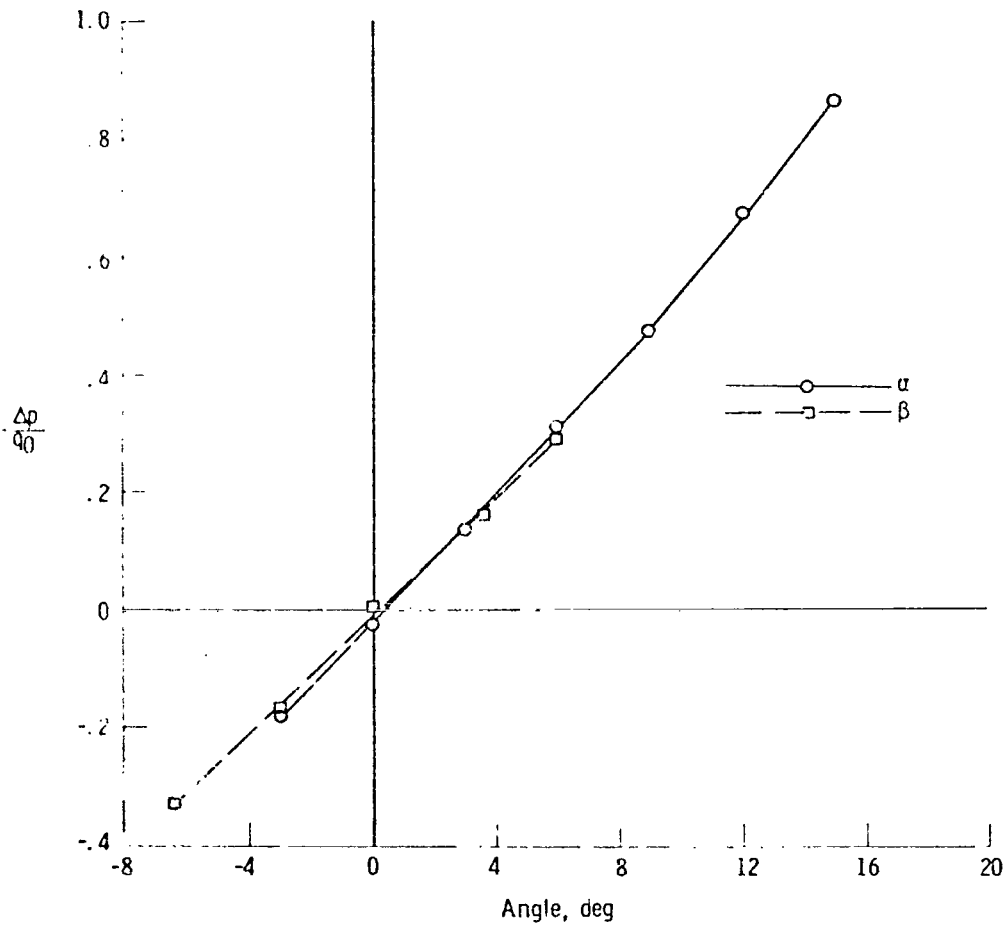
(a)  $M = 0.2$ ,  $N_{Re} = 4.92 \times 10^6$  per m ( $1.5 \times 10^6$  per ft).

Figure 5. Typical test sensor differential pressure coefficient versus boom angle data for sensor configuration A.



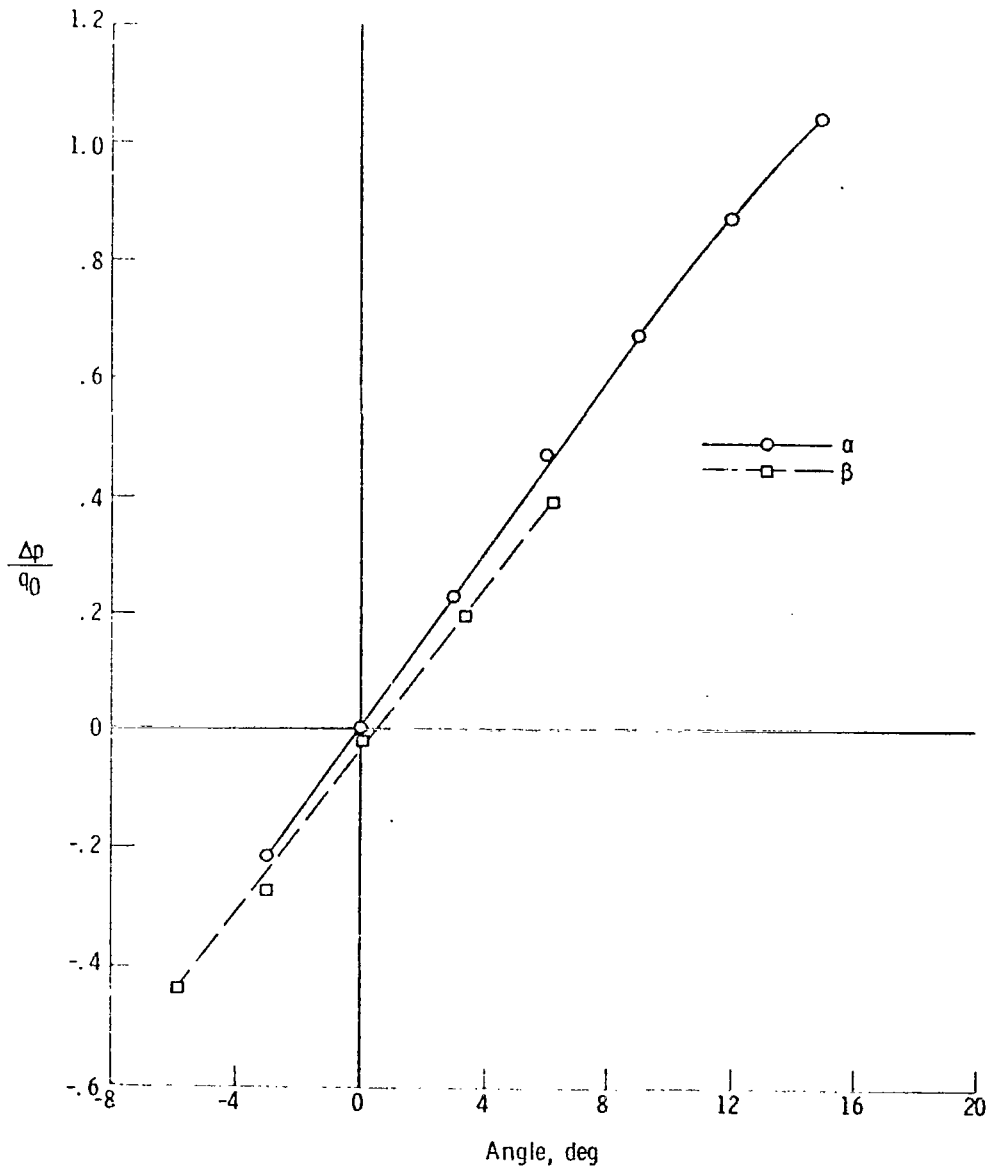
(b)  $M = 0.95$ ,  $N_{Re} = 26.2 \times 10^6$  per m ( $8.0 \times 10^6$  per ft).

Figure 5. Continued.



(c)  $M = 1.41$ ,  $N_{Re} = 26.2 \times 10^6$  per m ( $8.9 \times 10^6$  per ft).

Figure 5. Continued.



(d)  $M = 3.2$ ,  $N_{Re} = 26.2 \times 10^6$  per m ( $8.0 \times 10^6$  per ft).

Figure 5. Concluded.

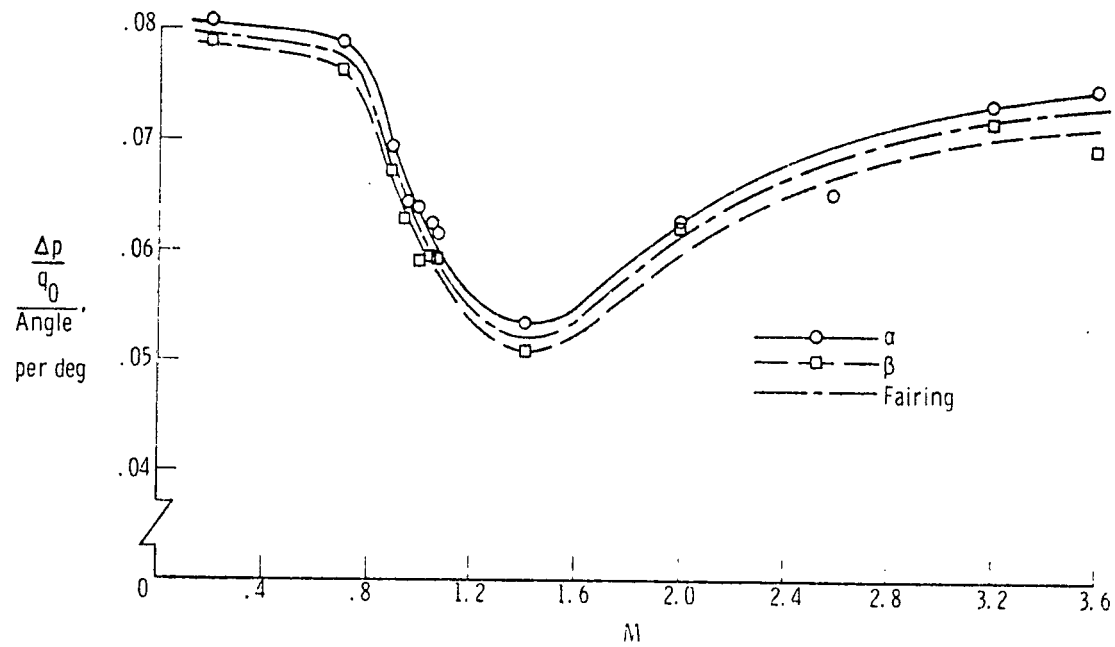


Figure 6. Sensitivity factor versus Mach number for sensor configuration A.  
 $N_{Re} = 4.92 \times 10^6$  per m to  $31.5 \times 10^6$  per m ( $1.5 \times 10^6$  per ft to  $9.6 \times 10^6$  per ft).

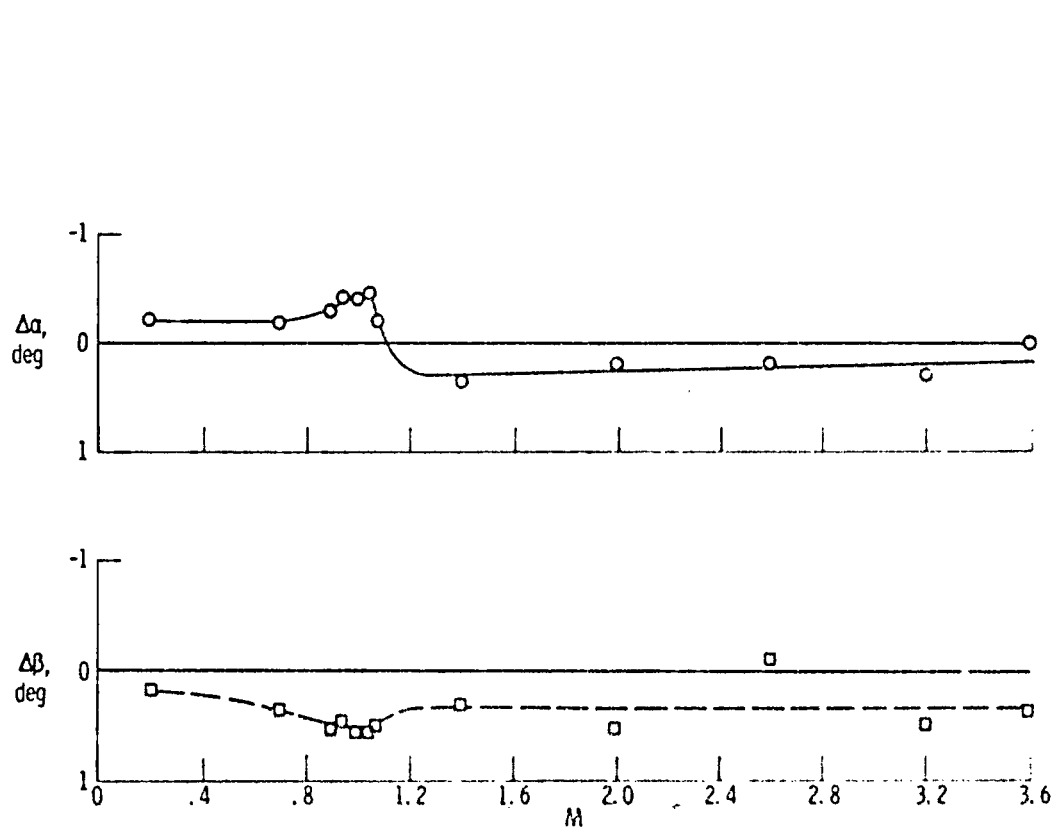
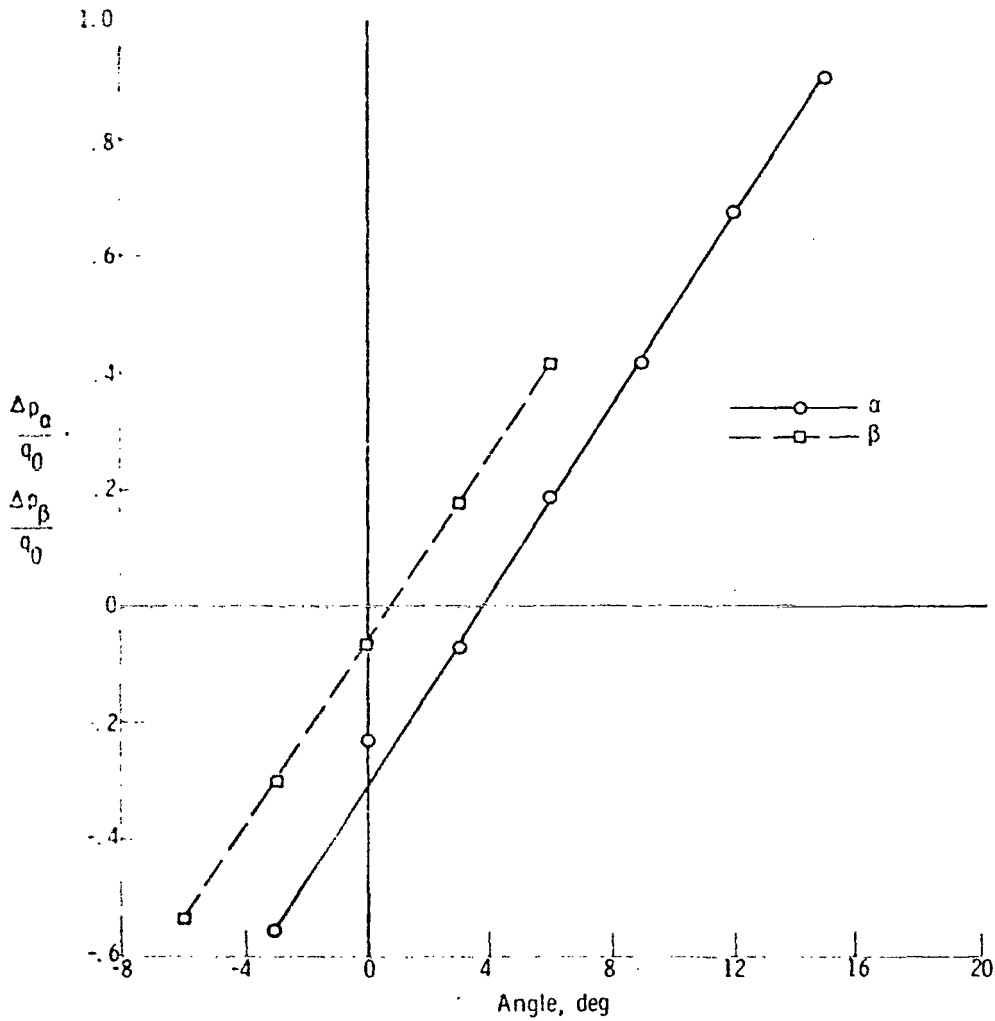
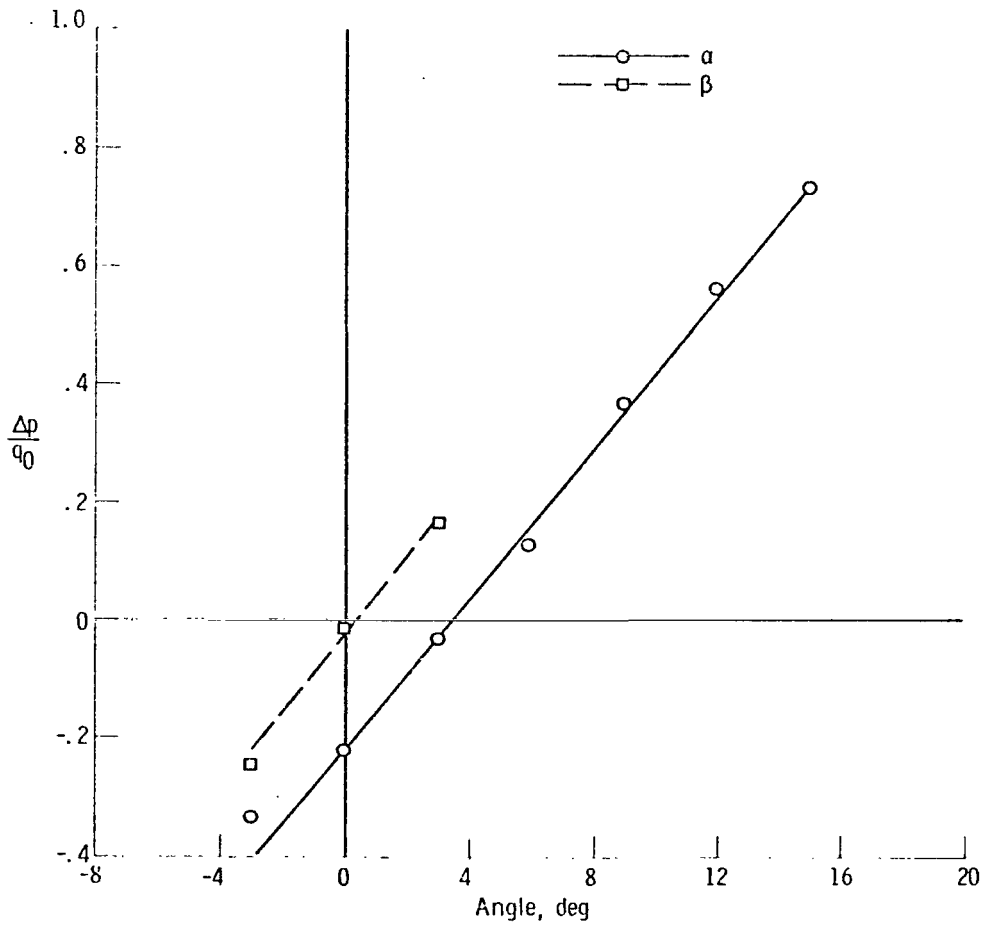


Figure 7. Incremental angles that correspond to the intersection point ( $\Delta P_{q_0} = 0$ ) for sensor configuration A.



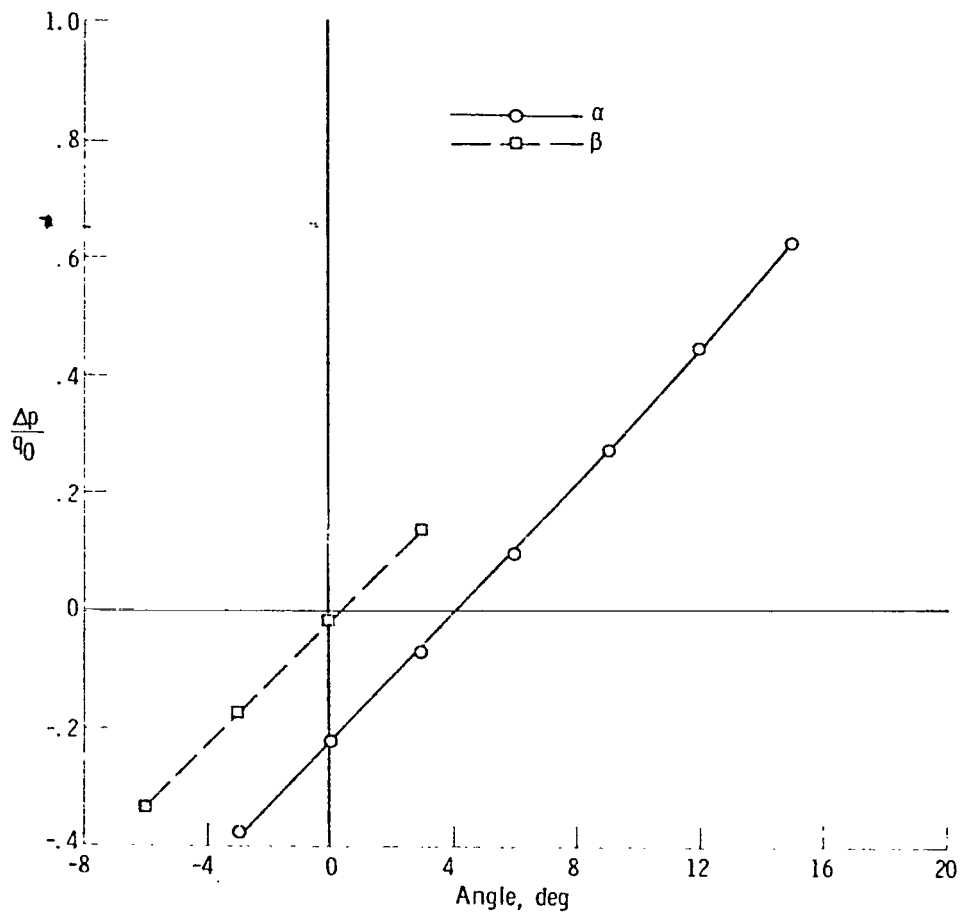
(a)  $M = 0.2$ ,  $N_{Re} = 4.92 \times 10^6$  per m ( $1.5 \times 10^6$  per ft).

Figure 8. Typical test sensor differential pressure coefficient versus boom angle data for sensor configuration B.



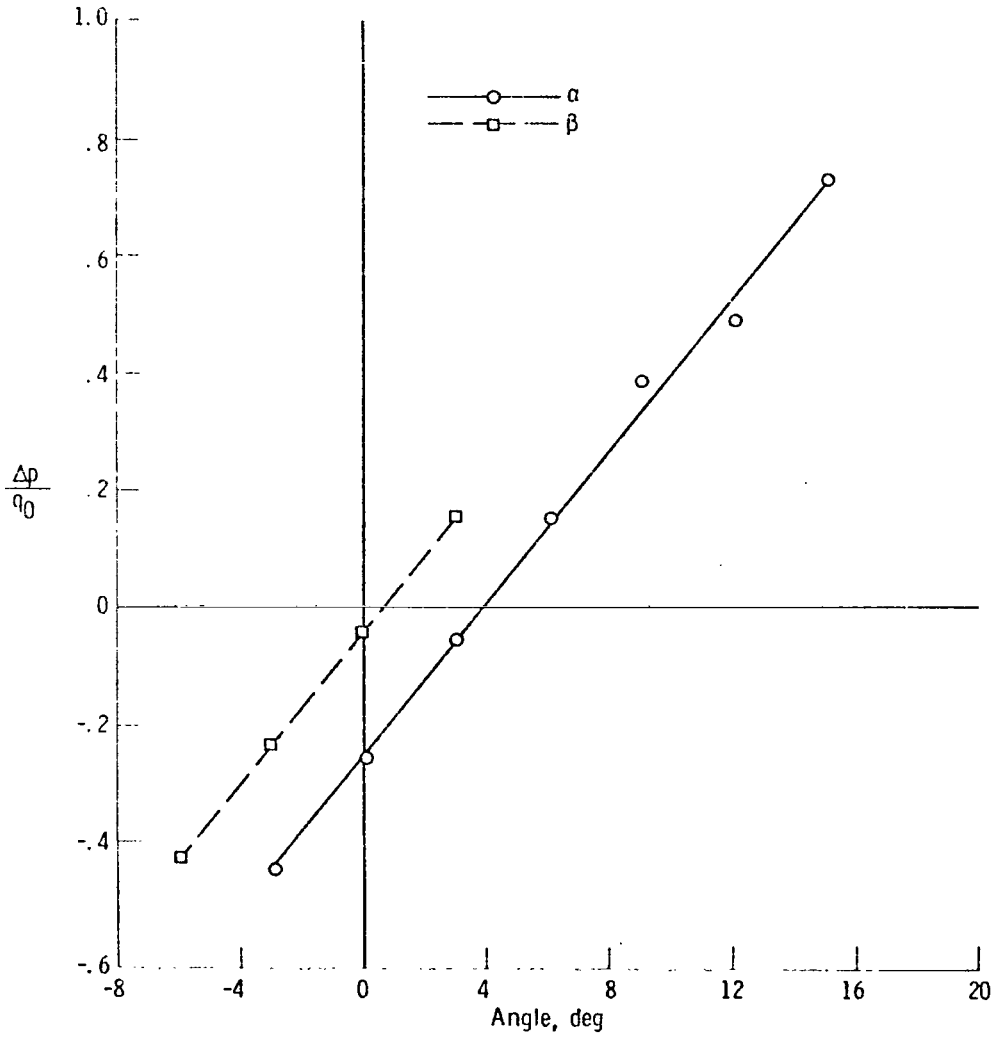
(b)  $M = 0.93$ ,  $N_{Re} = 13.1 \times 10^6$  per m ( $4.0 \times 10^6$  per ft).

Figure 8. Continued.



(c)  $M = 1.41$ ,  $N_{Re} = 13.1 \times 10^6$  per m ( $4.0 \times 10^6$  per ft).

Figure 8. Continued.



(d)  $M = 2.60$ ,  $N_{Re} = 13.1 \times 10^6$  per m ( $4.0 \times 10^6$  per ft).

Figure 8. Concluded.

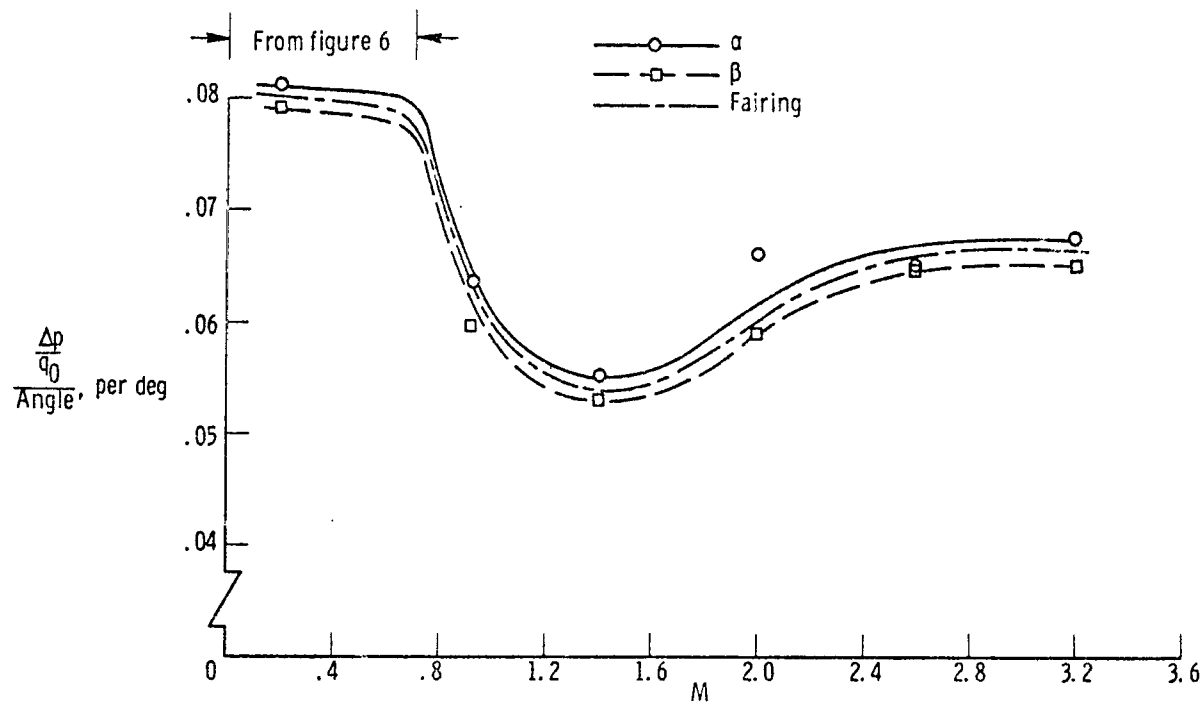


Figure 9. Sensitivity factor versus Mach number for sensor configuration B.  
 $N_{Re} = 4.92 \times 10^6$  per m to  $26.2 \times 10^6$  per m ( $1.5 \times 10^6$  per ft to  $8.0 \times 10^6$  per ft).

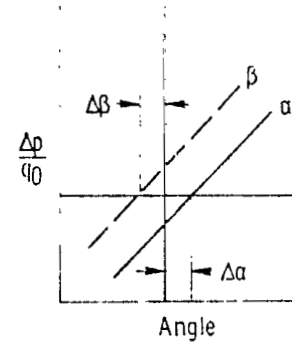
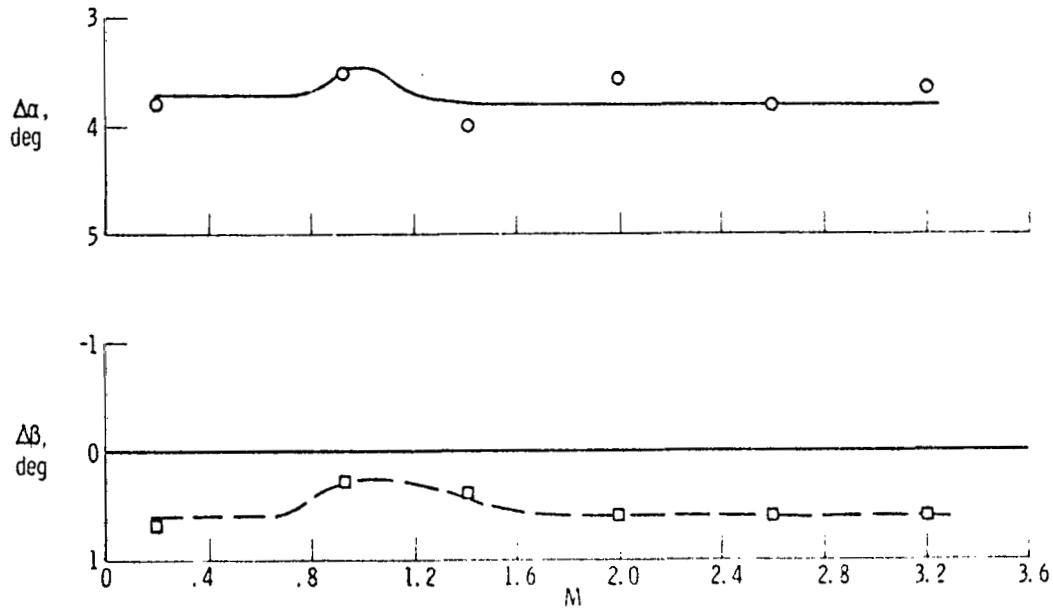
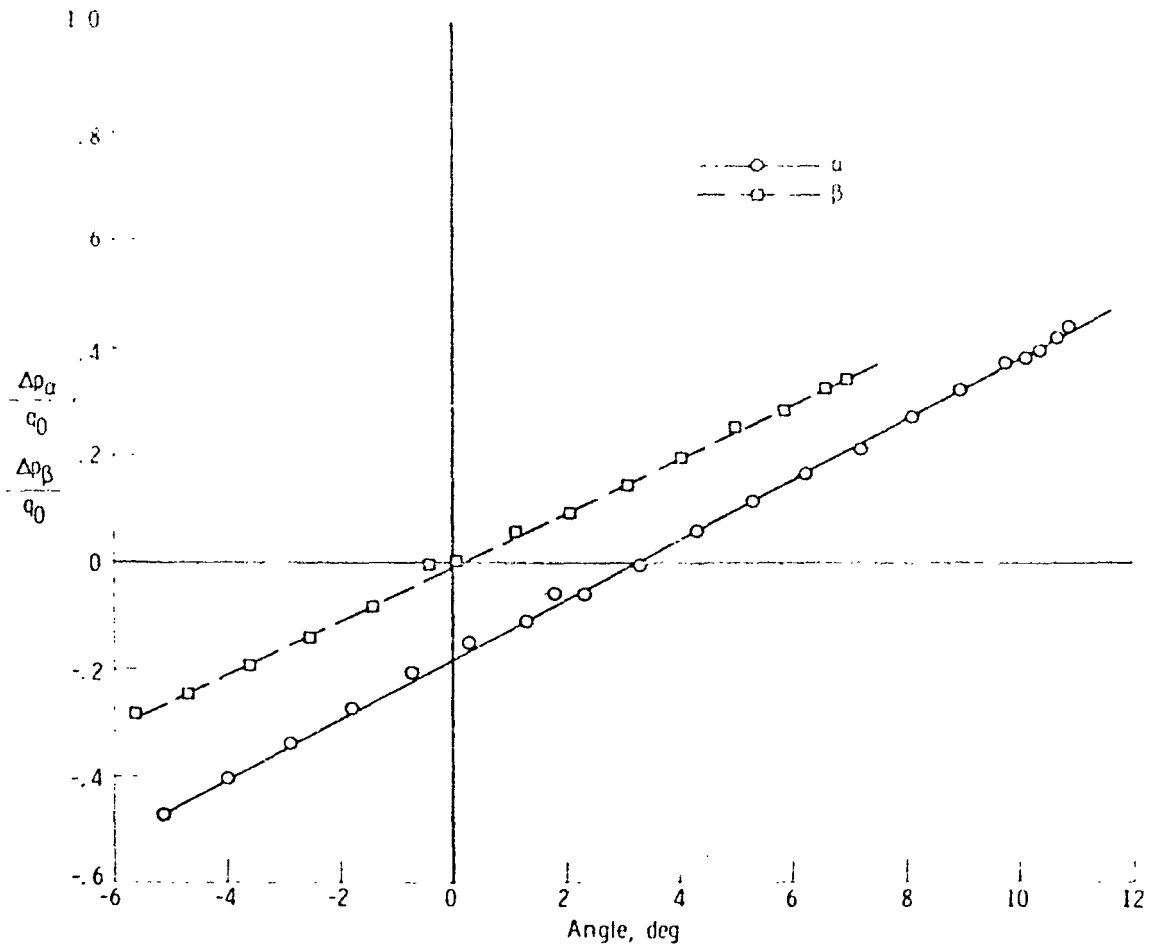
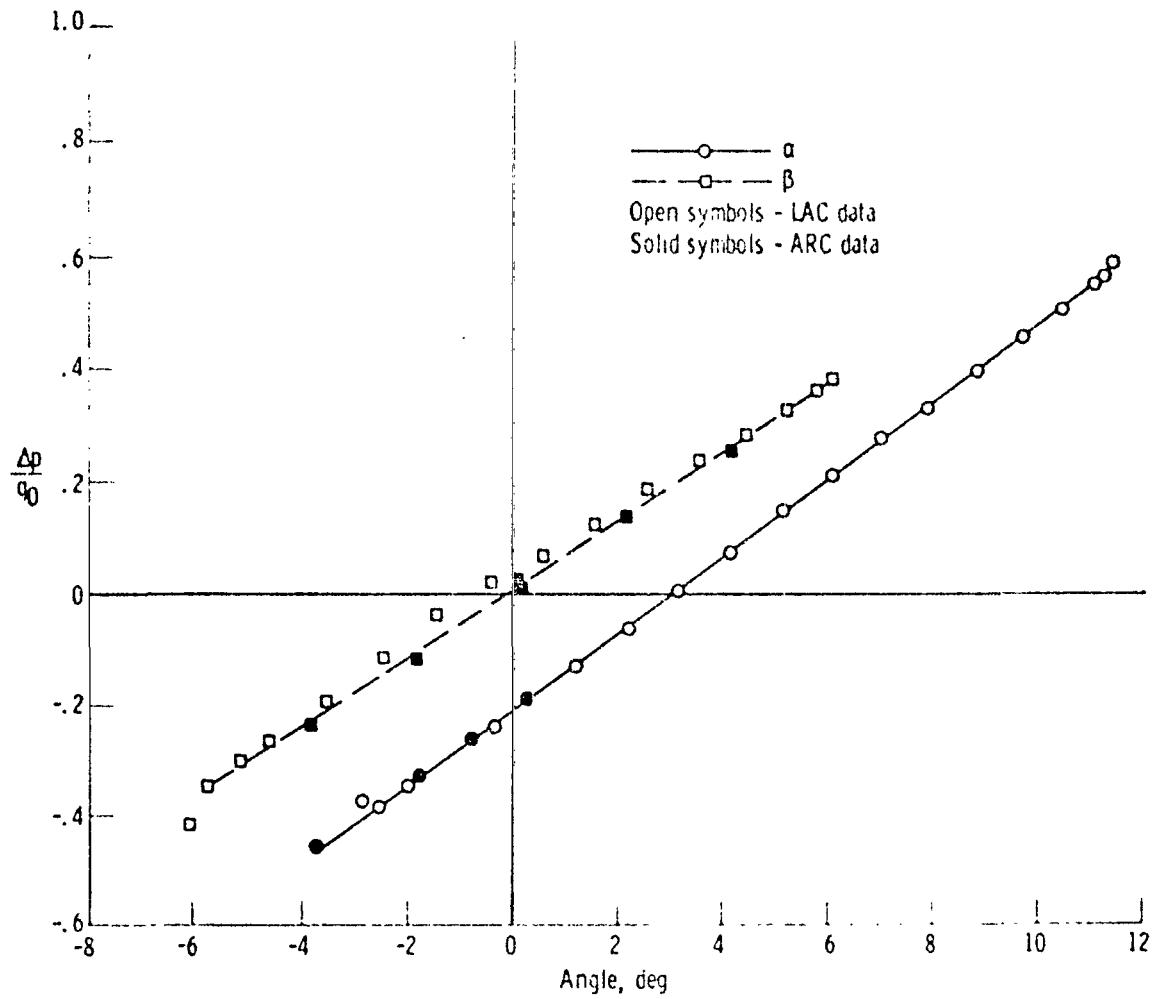


Figure 10. Incremental angles that correspond to the intersection point ( $\frac{\Delta p}{q_0} = 0$ ) for sensor configuration B.



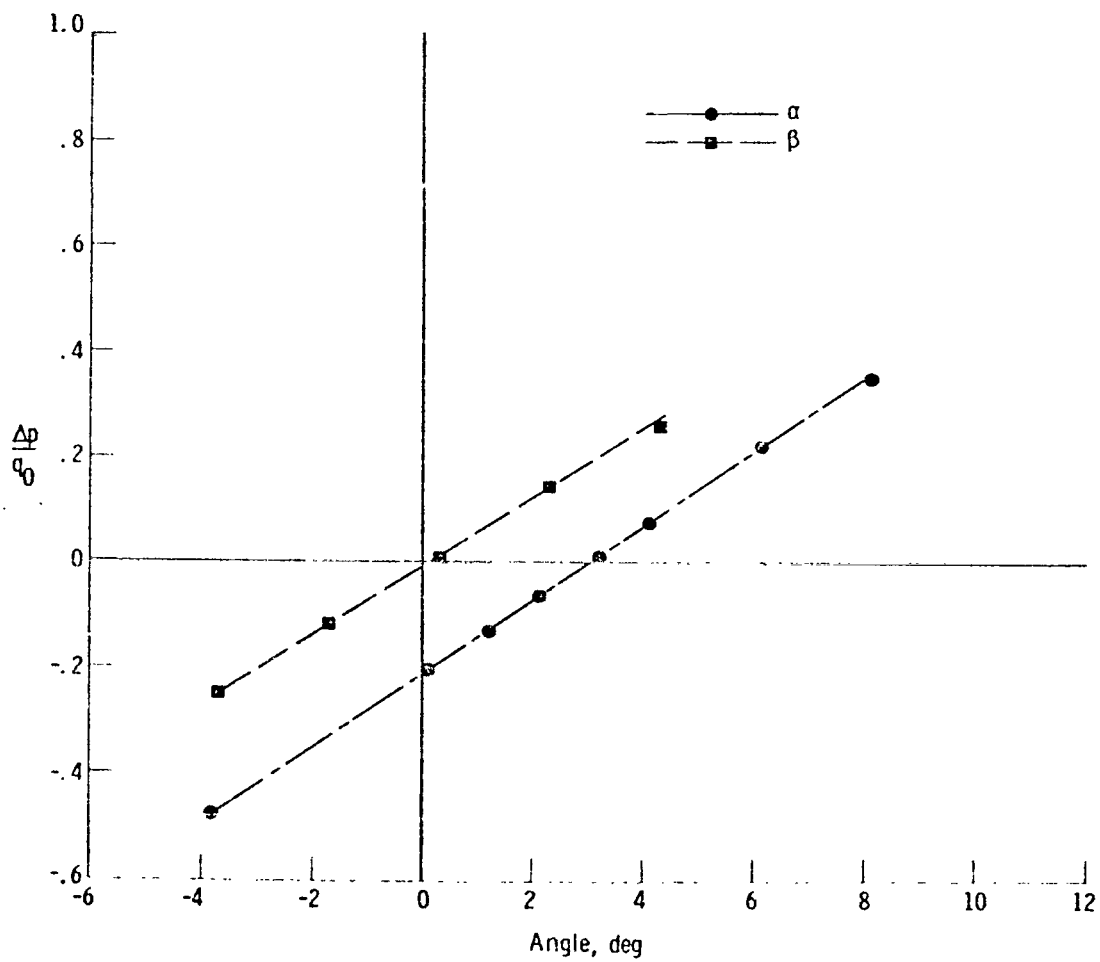
(a)  $M = 1.4$ ,  $N_{Re} = 24.3 \times 10^6$  per m ( $7.4 \times 10^6$  per ft).

Figure 11. Typical test sensor differential pressure coefficient versus boom angle data for sensor configuration C.



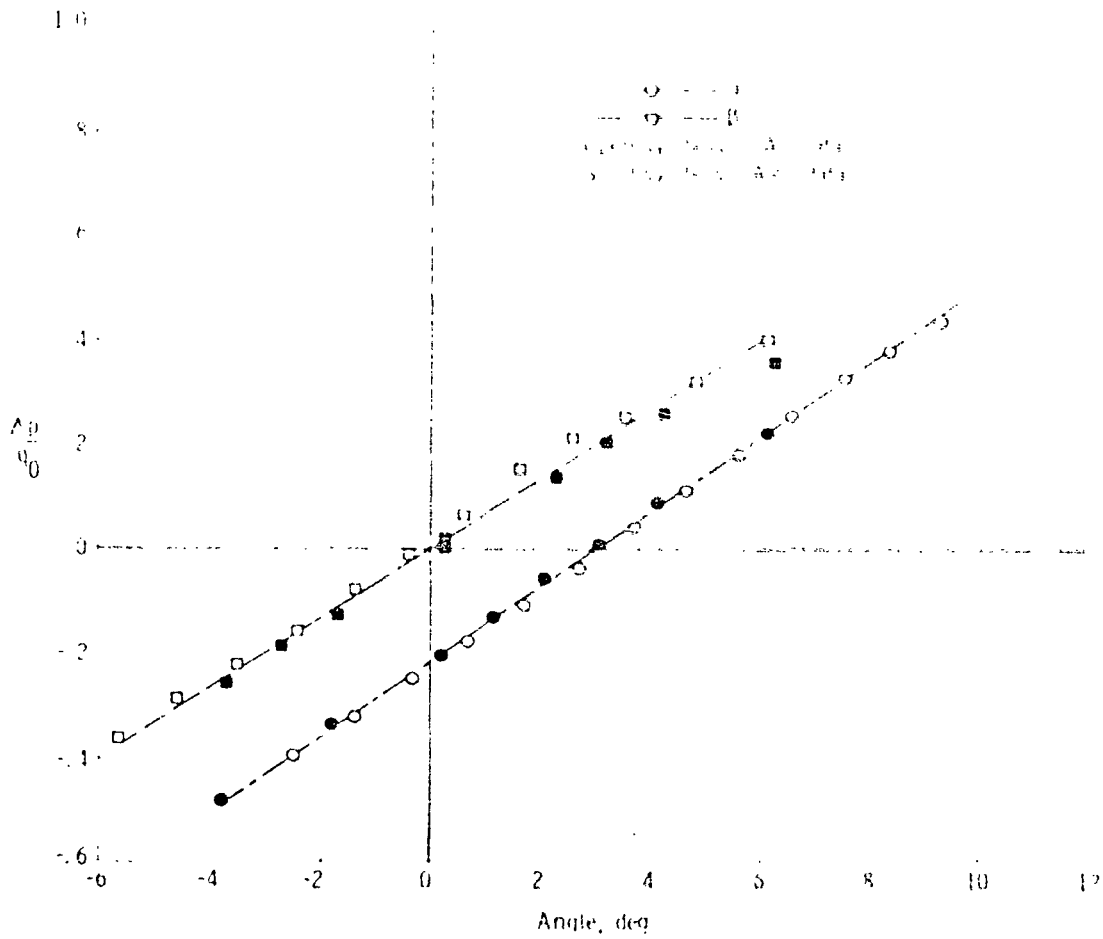
(b)  $M = 2.6$ ,  $N_{Re} = 38.7 \times 10^6$  per m ( $11.8 \times 10^6$  per ft) for LAC data and  $3.28 \times 10^6$  per m ( $1.0 \times 10^6$  per ft) for ARC data.

Figure 11. Continued.



(c)  $M = 3.0$ ,  $N_{Re} = 3.28 \times 10^6$  per m ( $1.0 \times 10^6$  per ft).

Figure 11. Continued.



(d)  $M = 3.2$ ,  $N_{Re} = 62.0 \times 10^6$  per m ( $18.9 \times 10^6$  per ft) for LAC data and  $3.28 \times 10^6$  per m ( $1.0 \times 10^6$  per ft) for ARC data.

Figure 11. Concluded.

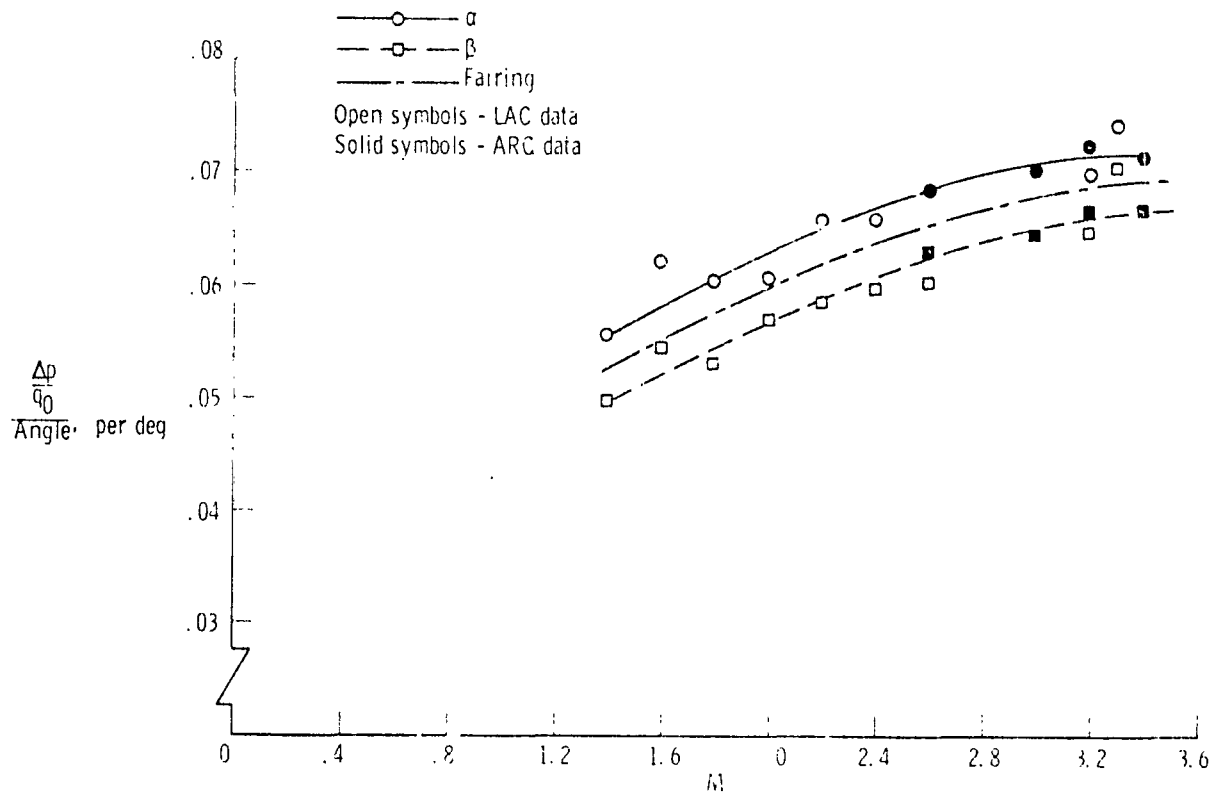


Figure 12. Sensitivity factor versus Mach number for sensor configuration C.  
 $N_{Re}$   $3.28 \times 10^6$  per m to  $65.6 \times 10^6$  per m ( $1.0 \times 10^6$  per ft to  $20 \times 10^6$  per ft).

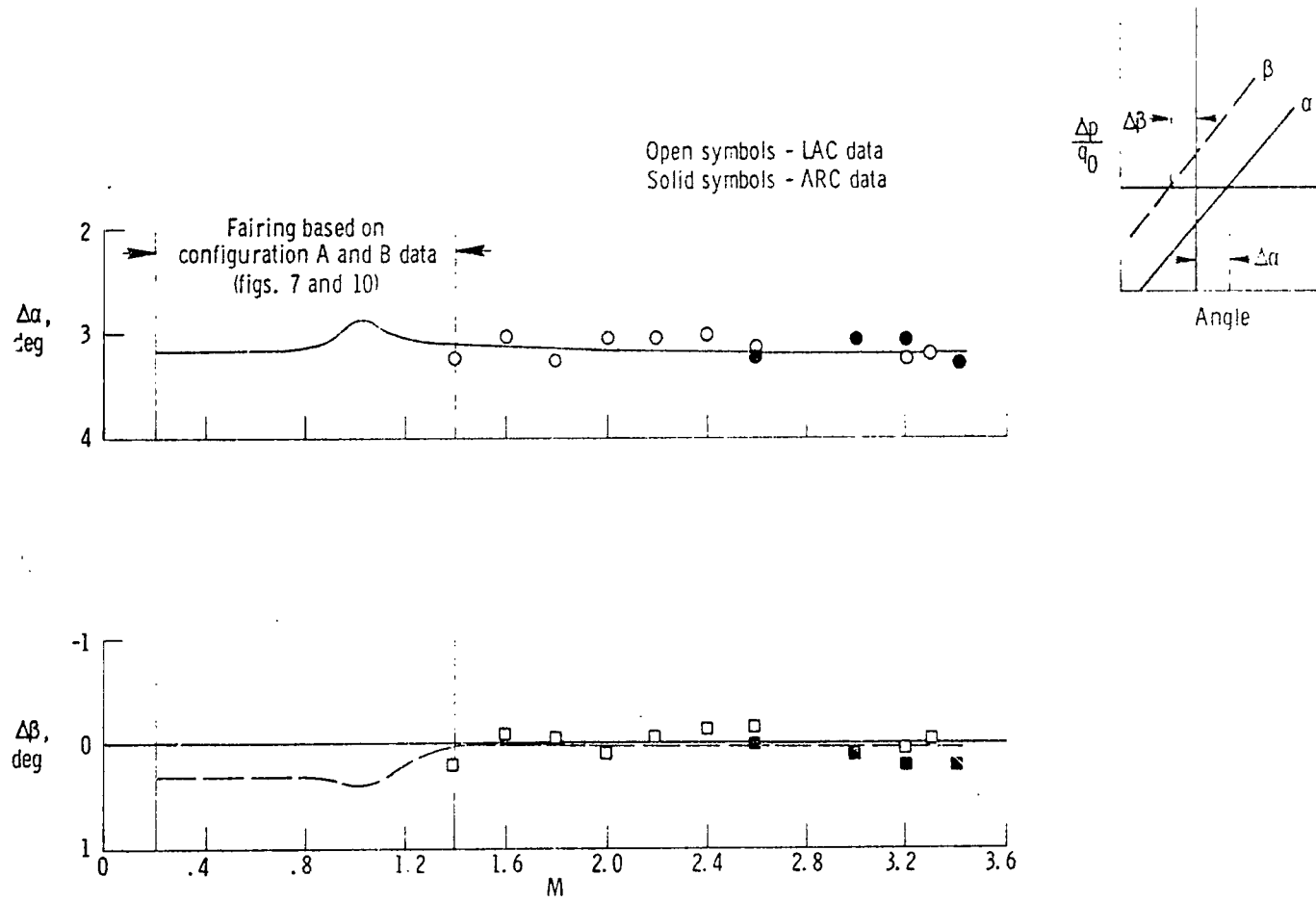
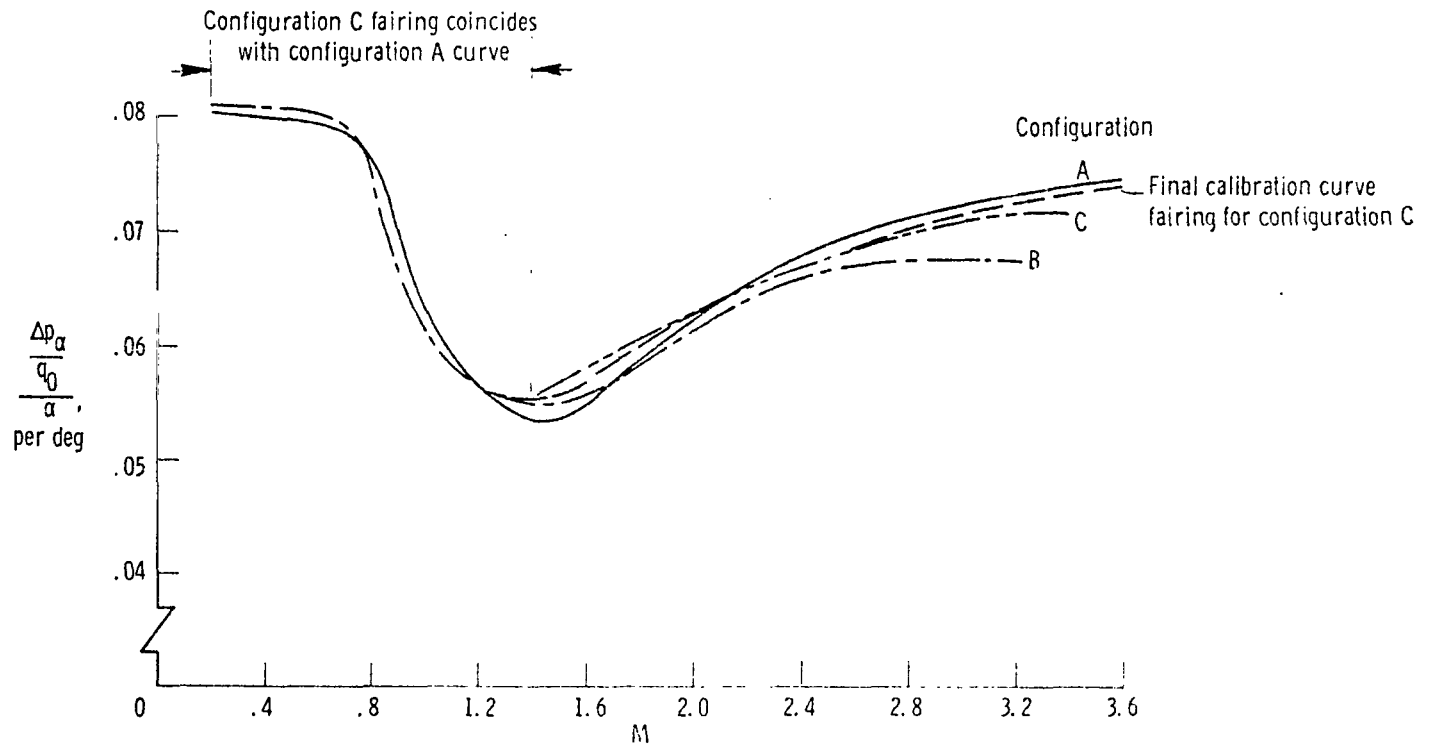
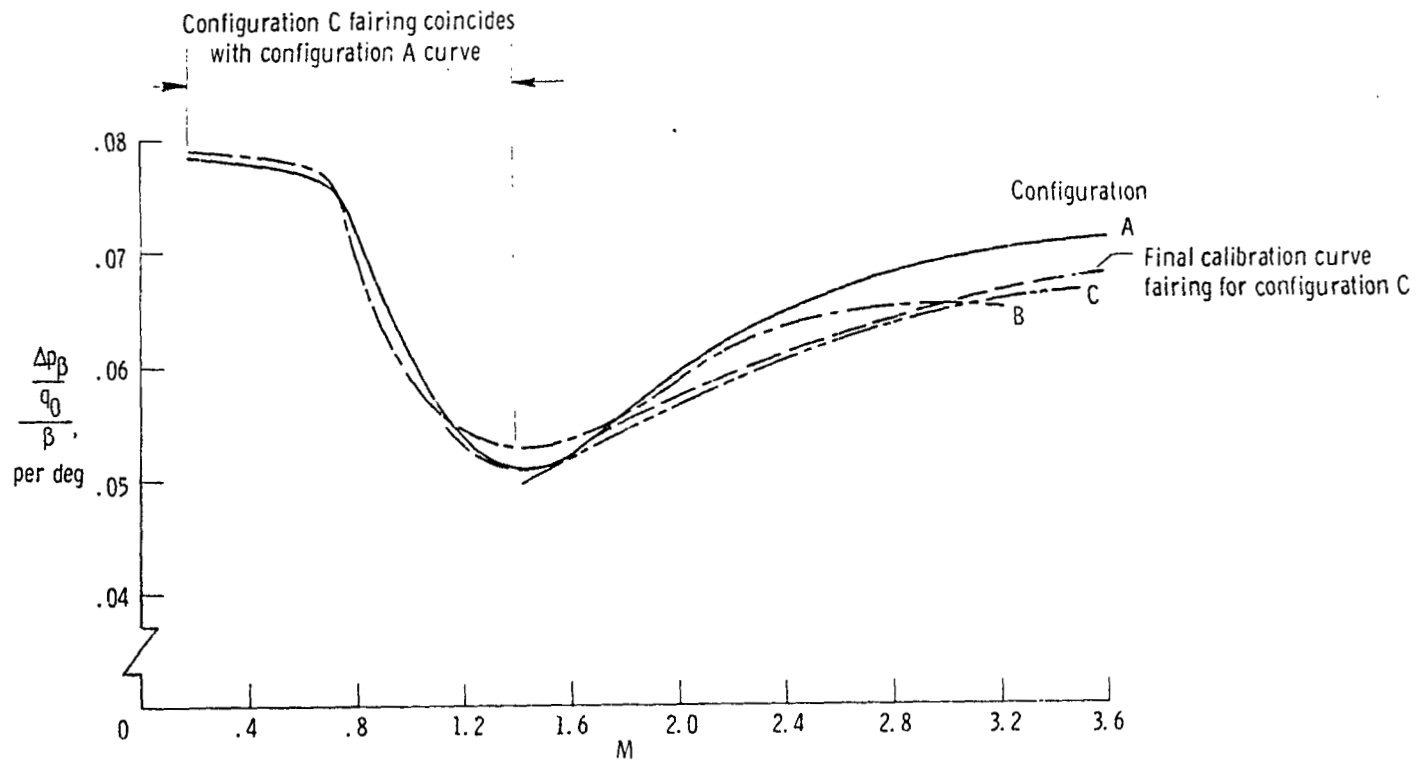


Figure 13. Incremental angles that correspond to the intersection point ( $\frac{\Delta p}{q_0} = 0$ ) for sensor configuration C.



(a) Angle of attack.

Figure 14. Comparison of wind-tunnel sensitivity factor versus Mach number for sensor configurations A, B, and C.



(b) Angle of sideslip.

Figure 14. Concluded.

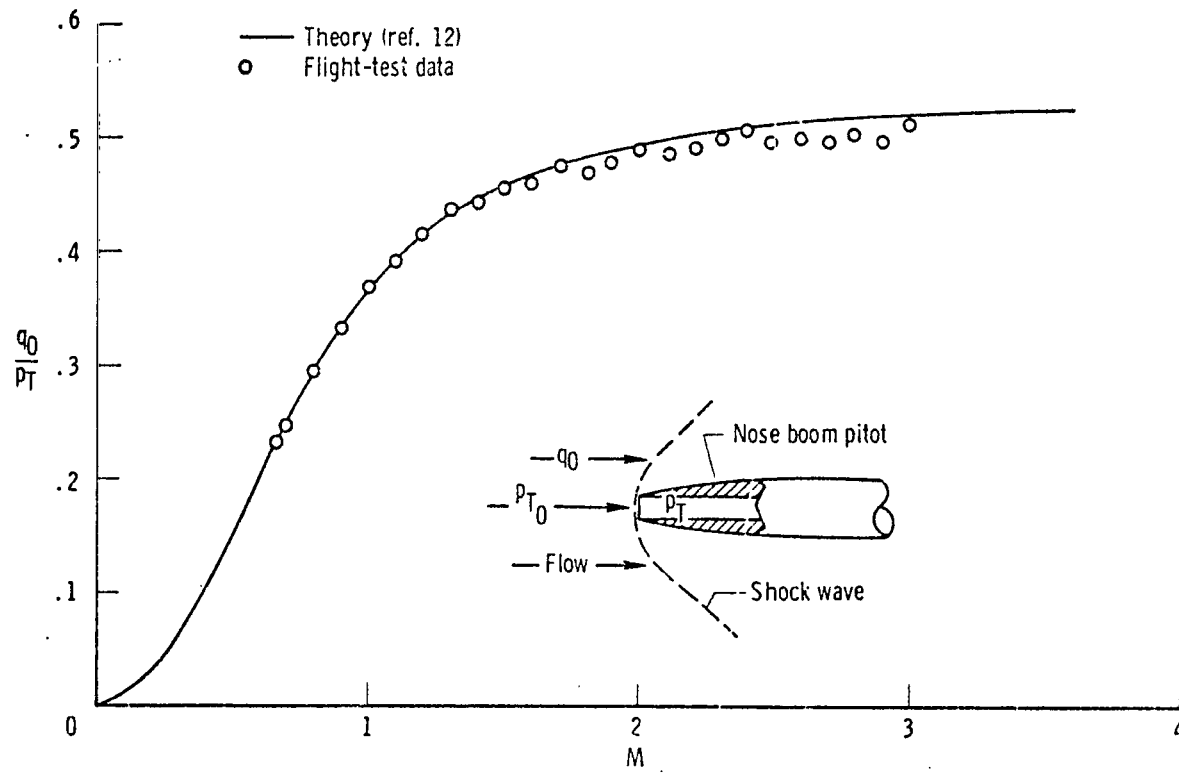


Figure 15. Comparison of flight and theoretical  $\frac{q_0}{p_T}$  data as a function of Mach number.

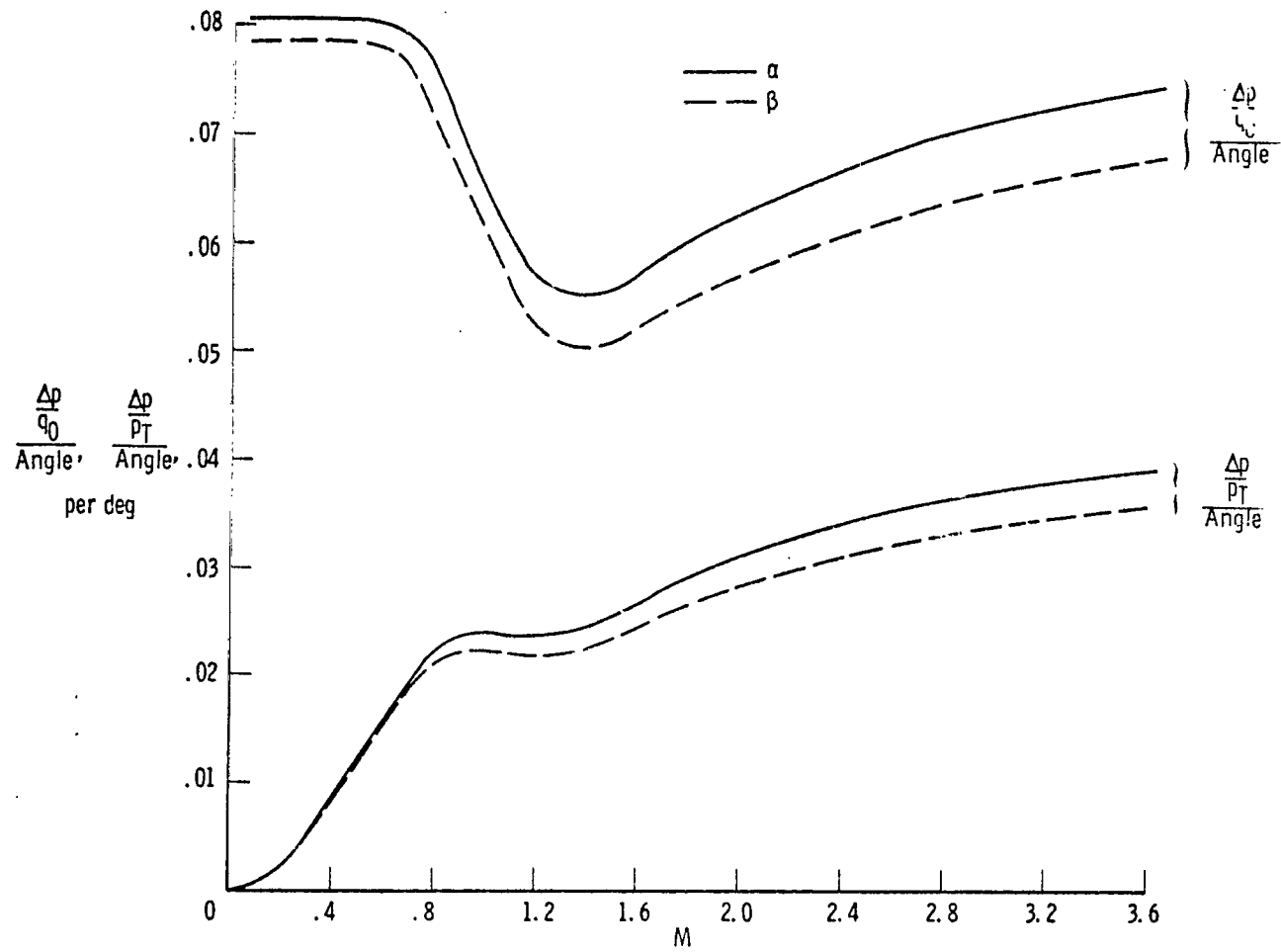


Figure 16. Slope calibrations for configuration C in terms of  $\frac{\Delta p}{q_0}$  and  $\frac{\Delta p}{p_T}$  as a function of Mach number.

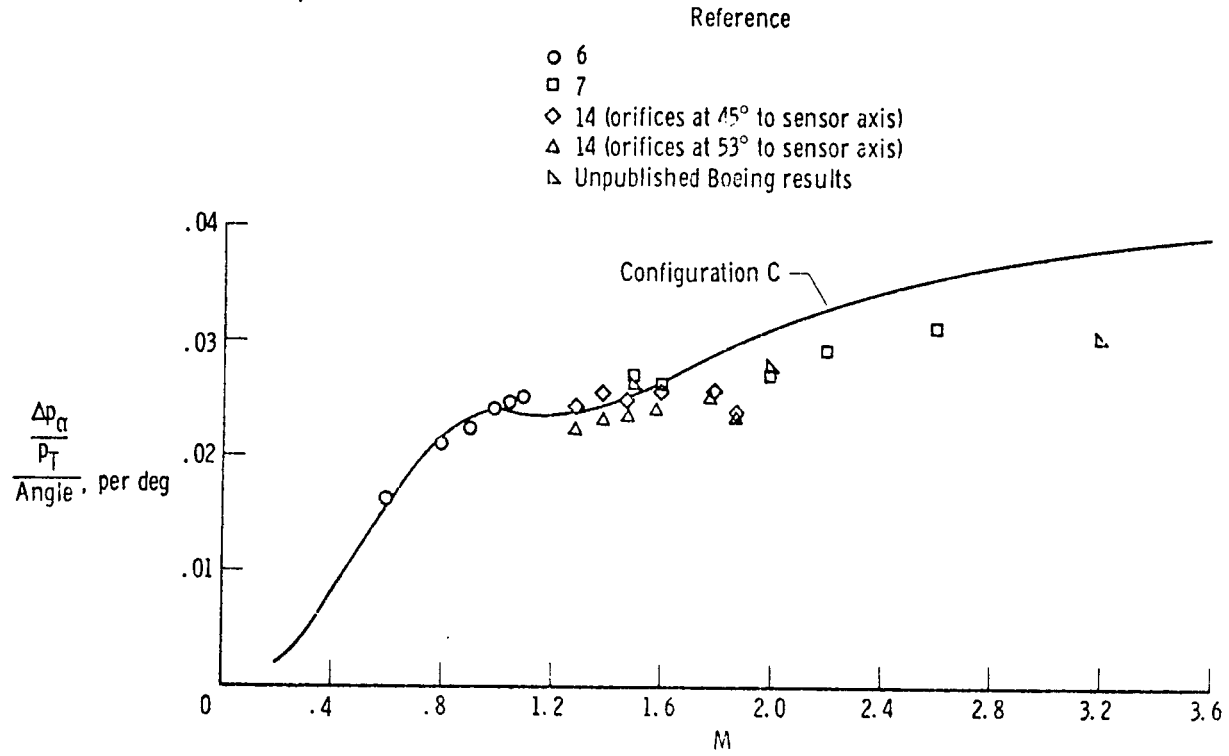


Figure 17. Comparison of isolated hemispherical head sensor results from various studies with configuration C results.

**END**

**DATE**

**FILMED**

**APR 20 1973**